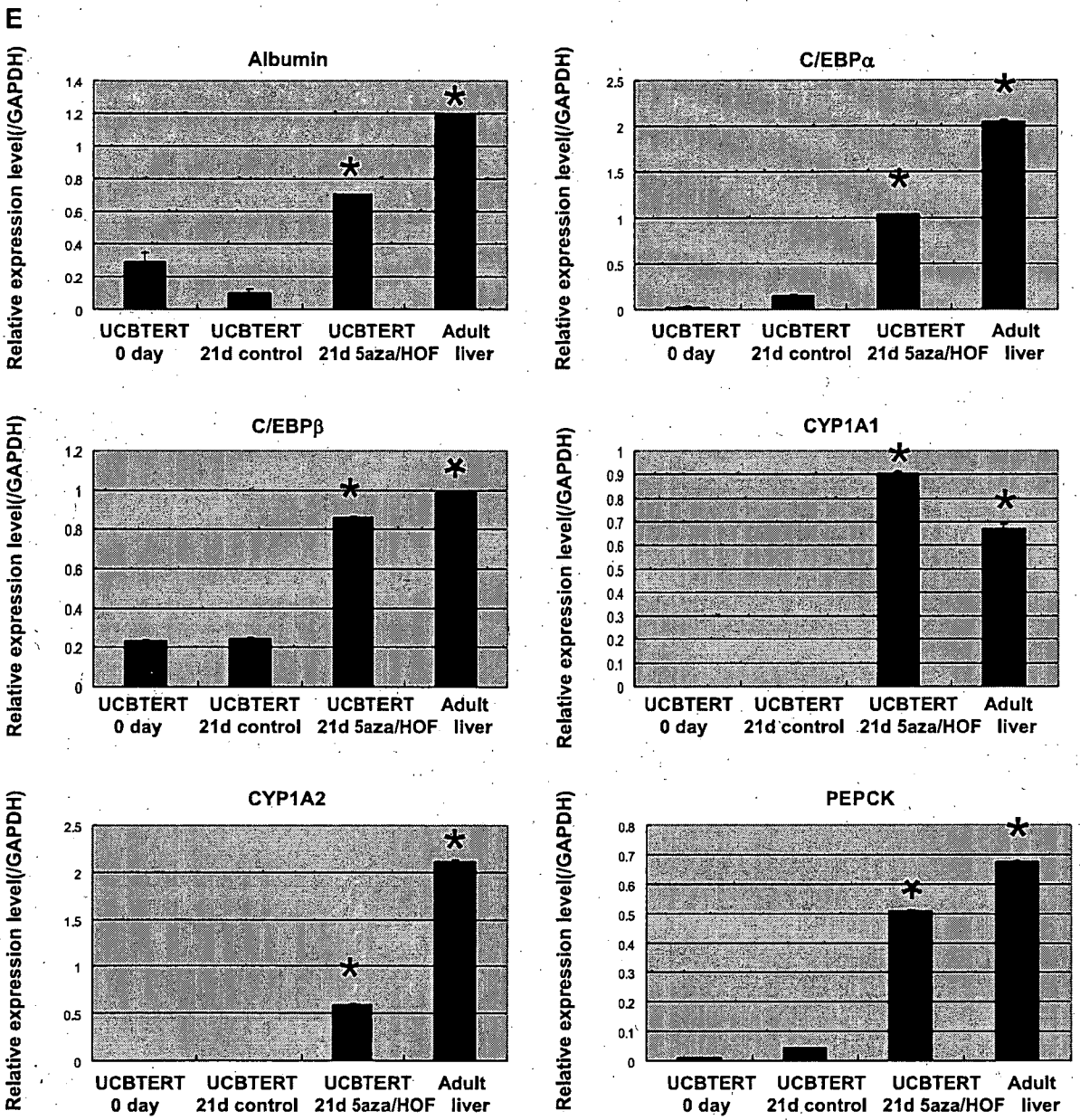

Fig. 2—*Continued. E*: expression of hepatocyte-specific genes in 5-aza/HGF/OSM/FGF2-treated cells compared with human adult normal liver. Hepatocyte-specific genes included albumin, C/EBPα, C/EBPβ, CYP1A1, CYP1A2, and phosphoenolpyruvate carboxykinase (PEPCK). PEPCK is the rate-limiting enzyme of glucogenesis. UCBTERT *day 0*, UCBTERT 21d control, UCBTERT 21d 5-aza/HOF, and Adult liver represent UCBTERT cells before incubation, cells incubated in 10% FBS for 21 days, cells incubated in 5-aza/HGF/OSM/FGF2 for 21 days, and adult liver tissue, respectively. Data are expressed as means ± SE of 3 experiments. $*P < 0.05$, compared with UCBTERT *day 0*.

whereas the luciferase activity in the cells transfected with Fz8-siRNA was 25% of that in the cells transfected with control siRNA, indicating that Wnt/β-catenin signaling was suppressed by transfection with Fz8-siRNA (Fig. 4*C*). Because the suppressive effect of transfection with lipofection reagent did not last more than 7 days (data not shown), transfection with Fz8-siRNA was repeated every 7 days. Weekly transfection of Fz8-siRNA caused an increase in albumin mRNA expression in UCBTERT-21 cells on *day 14* and *day 21*, as observed in UCBTERT-21 cells treated with 5-aza and cytokines (Fig. 4*D*).

UCBTERT-21 cells 3 wk after the beginning of Fz8-siRNA treatment were examined for hepatic marker proteins. Suppression of Fz8 by siRNA transfection induced the expression of albumin, C/EBPα, and CYP1A1/2 in UCBTERT-21 cells (Fig. 4*E*). The UCBTERT-21 cells treated with Fz8-siRNA were rounder than those subjected to "hepatic induction treatment." The numbers of albumin-, C/EBPα-, CYP1A1/2-, and PAS-

Table 1. *Microarray analysis of Wnt signal-related genes*

Name	Description	Accession Number	Ratio
CTNNB1	catenin (cadherin-associated protein), beta 1 (88kd); ctnnb1	NM_001904	0.409285785
CTNNBIP1	beta-catenin-interacting protein icat; ctnnbip1	NM_020248	2.445343626
FZ1	frizzled 1; fzd1	NM_003505	0.664559843
FZ2	frizzled-2; fzd2	AB017364	1.302192999
FZ3	frizzled homolog 3; fzd3	AJ272427	0
FZ3	frizzled homolog 3 (*Drosophila*); fzd3	NM_017412	0
FZ4	frizzled homolog 4 (*Drosophila*); fzd4	NM_012193	0.815346448
FZ5	frizzled 5; fzd5	NM_003468	0
FZ6	frizzled 6; fzd6	NM_003506	0
FZ7	frizzled 7; fzd7	NM_003507	0.800848224
FZ8	seven-transmembrane receptor frizzled-8; fzd8	AB043703	0.479522821
FZ9	frizzled 9; fzd9	NM_003508	0
FZ10	frizzled homolog 10 (*Drosophila*); fzd10	NM_007197	0.662549833
PPP2CA	protein phosphatase 2 (formerly 2a), catalytic subunit, alpha isoform; ppp2ca	NM_002715	0.177625911
PPP2CB	protein phosphatase 2 (formerly 2a), catalytic subunit, beta isoform; ppp2cb	NM_004156	0.642124376
PPP2R1A	protein phosphatase 2 (formerly 2a), regulatory subunit a (pr 65), alpha isoform; ppp2r1a	NM_014225	0.89013334
PPP2R1B	protein phosphatase 2 (formerly 2a), regulatory subunit a (pr 65), beta isoform; ppp2r1b	NM_002716	2.005757068
SFRP1	secreted apoptosis related protein 2; sarp2	AF017987	0.849458445
SFRP2	similar to stromal cell derived factor 5	BC008666	0
SFRP4	secreted frizzled-related protein 4; sfrp4	NM_003014	1.937534515
WNT1	wingless-type mmtv integration site family, member 1 precursor; wnt1	NM_005430	0
WNT2	ensemble prediction	ENSG00000105989	0.96735482
WNT2B	wingless-type mmtv integration site family, member 2b, isoform wnt-2b1; wnt2b	NM_004185	0
WNT2B	wingless-type mmtv integration site family, member 2b, isoform wnt-2b2; wnt2b	NM_024494	0
WNT4	wnt4 precursor; wnt4	AY009398	0.900795213
WNT5A	wingless-type mmtv integration site family, member 5a precursor; wnt5a	NM_003392	0
WNT6	similar to wingless-related mmtv integration site 6	BC004329	0
WNT7A	wingless-type mmtv integration site family, member 7a precursor; wnt7a	NM_004625	0
WNT8B	wingless-type mmtv integration site family, member 8b precursor; wnt8b	NM_003393	1.052495538
WNT9A	wnt14	AB060283	0.47555091
WNT9B	wnt-like protein wnt15; wnt15	AF028703	0
WNT10A	wingless-type mmtv integration site family, member 10a precursor; wnt10a	NM_025216	0
WNT10B	wingless-type mmtv integration site family, member 10b precursor; wnt10b	NM_003394	1.247761639
WNT11	wingless-type mmtv integration site family, member 11 precursor; wnt11	NM_004626	0
WNT16	wingless-type mmtv integration site family, member 16, isoform 2; wnt16	NM_016087	0.911155662

positive cells increased by 3.2-fold, 3-fold, 1.7-fold, and 6-fold, respectively (each, $P < 0.01$, Fig. 4*F*). However, there was no significant change in urea synthesis when the cells were transfected with Fd8-siRNA (data not shown).

The subcellular distribution of β-catenin in UCBTERT-21 cells transfected with Fz8-siRNA was investigated by immunocytochemistry. β-Catenin was located along the cell membrane and in the cytoplasm of the cells transfected with Fz8-siRNA (Fig. 4*G*).

DISCUSSION

In the present study, we identified an important signal for hepatic fate specification by using a system to induce hepatocytes to differentiate from human UCBMSCs. The combination of HGF, OSM, and FGF2 was examined, since the receptors for these cytokines were highly expressed on UCBTERT-21 cells (data not shown). In addition, during embryonic development, the production of growth factors such as HGF and FGFs has been associated with endoderm specification (40, 16). Furthermore, the first event that occurs after acute hepatitis in humans is a large increase in the serum level of HGF (42), suggesting that HGF plays an important role in the early stages of hepatogenesis. 5-Aza was employed because its efficiency in terms of cardiomyogenic differentiation of murine bone marrow stromal cells was ~30% (29). There is now evidence that the remodeling of chromatin and the alterations of epigenetics, including histone methylation and acetylation and DNA methylation, can cause committed cells to convert from one fate to another (6, 19). In our preliminary experiment, trichostatin A, a histone deacetylase inhibitor, induced apoptosis, but not differentiation, of UCBTERT-21 cells. Hence trichostatin A was not used in the present study. The positive rates of albumin, C/EBPα, CYP1A1/2, and PAS staining were not identical. This phenomenon may be explained by differences in the sensitivity of the immunostaining. In addition, the hierarchy of expression of liver-enriched transcription factors and proteins during development may explain this discrepancy (48).

Human UCBMSCs are easy to isolate but difficult to study because of their limited life span. The advantages of using UCBTERT-21 cells in a repopulation study are as follows: the cells have the same expression pattern of surface markers as the parental cells, the cells displayed osteogenic and adipogenic differentiation, the cells do not transform, they do not generate tumors in immunosuppressed mice, they do not form foci in vitro, and they stop dividing when confluent (46). Although important concerns regarding the use of these "artificial" cells, into which the hTERT genes has been introduced, for human liver repopulation studies may be raised, the use of UCBTERT-21 cells meets the purpose of the present study. In addition, the use of these cells enabled us to demonstrate the reversibility of differentiation. Therefore, to establish an effi-

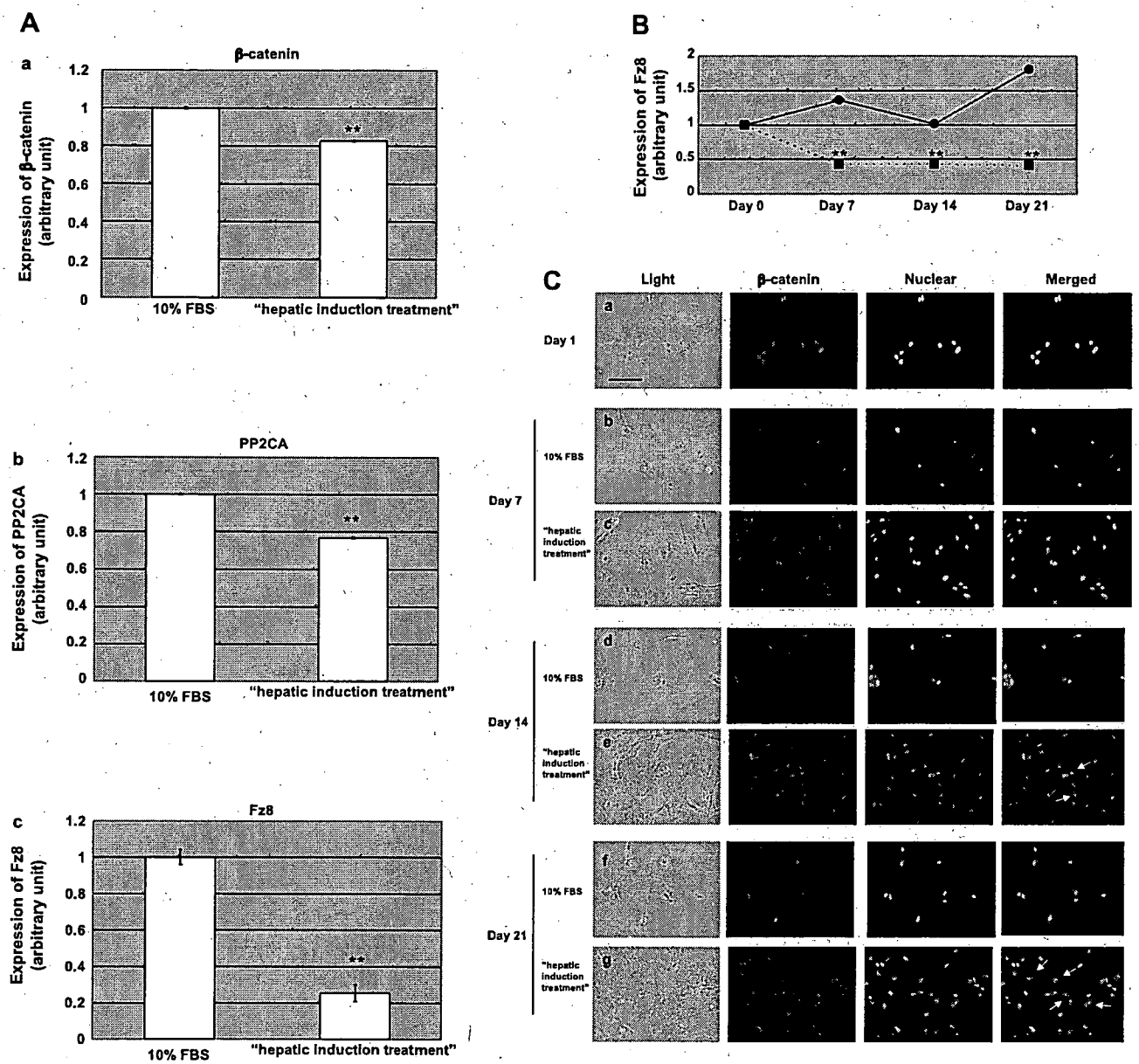

Fig. 3. Downregulation of Wnt/β-catenin genes during hepatic differentiation of UCBTERT-21 cells. *A*: mRNA levels of Wnt/β-catenin signaling genes at *day 21* of control and 5-aza/HGF/OSM/FGF2 treatment as assessed by real-time RT-PCR. Expression levels of the β-catenin (*a*), PP2CA (*b*), and Fz8 (*c*) genes are expressed as a ratio of the control treatment. Data are expressed as means ± SE of 3 experiments. $^{**}P < 0.01$, compared with control. *B*: expression of Fz8 mRNA on *days 0*, *7*, *14*, and *21* was assessed by real-time RT-PCR. The level of Fz8 is expressed as a ratio of that on *day 0*. ●, 10% FBS (control); ■, 5-aza/HGF/OSM/FGF2. Data are expressed as means ± SE of 3 experiments. $^{**}P < 0.01$, compared with control. *C*: localization of β-catenin in UCBTERT-21 cells during hepatic differentiation. *a*, *b*, *d*, and *f*, 10% FBS (control); *c*, *e*, and *g*, 10% FBS with 5-aza/HGF/OSM/FGF2. Light micrograph (Light), β-catenin staining (β-catenin), nuclear staining (Nuclear), and merged images of β-catenin and nuclear staining (Merged) are shown. SYTOX green was utilized for nuclear staining. β-Catenin was located in the cytoplasm (arrows) of several differentiated cells. Scale bar, 100 μm.

cient induction treatment, tissue engineers might apply this protocol to primary cultured human MSCs, which have not been genetically manipulated.

Recent studies have demonstrated that the Wnt/β-catenin signal plays a crucial role in the regulation of stem cell functions (17). Wnt signaling maintains the self-renewing properties of hematopoietic stem cells and pluripotency of embryonic stem cells (37, 39). In addition to promoting the proliferation of stem/progenitor cells, Wnt also influences the lineage adopted by stem cells. A requirement for Wnt signaling was observed for neuronal specification in the dorsal spinal cord (33). β-Catenin-deficient mouse stem cells fail to differentiate into follicular keratinocytes and instead adopt an epidermal fate (12).

The expression of the gene encoding a Wnt antagonist, Secreted frizzled-related protein 5 (sFRP5), in the foregut endoderm gave rise to the liver in mouse and *Xenopus* (10, 35), suggesting that the Wnt signal is a negative regulator of hepatic

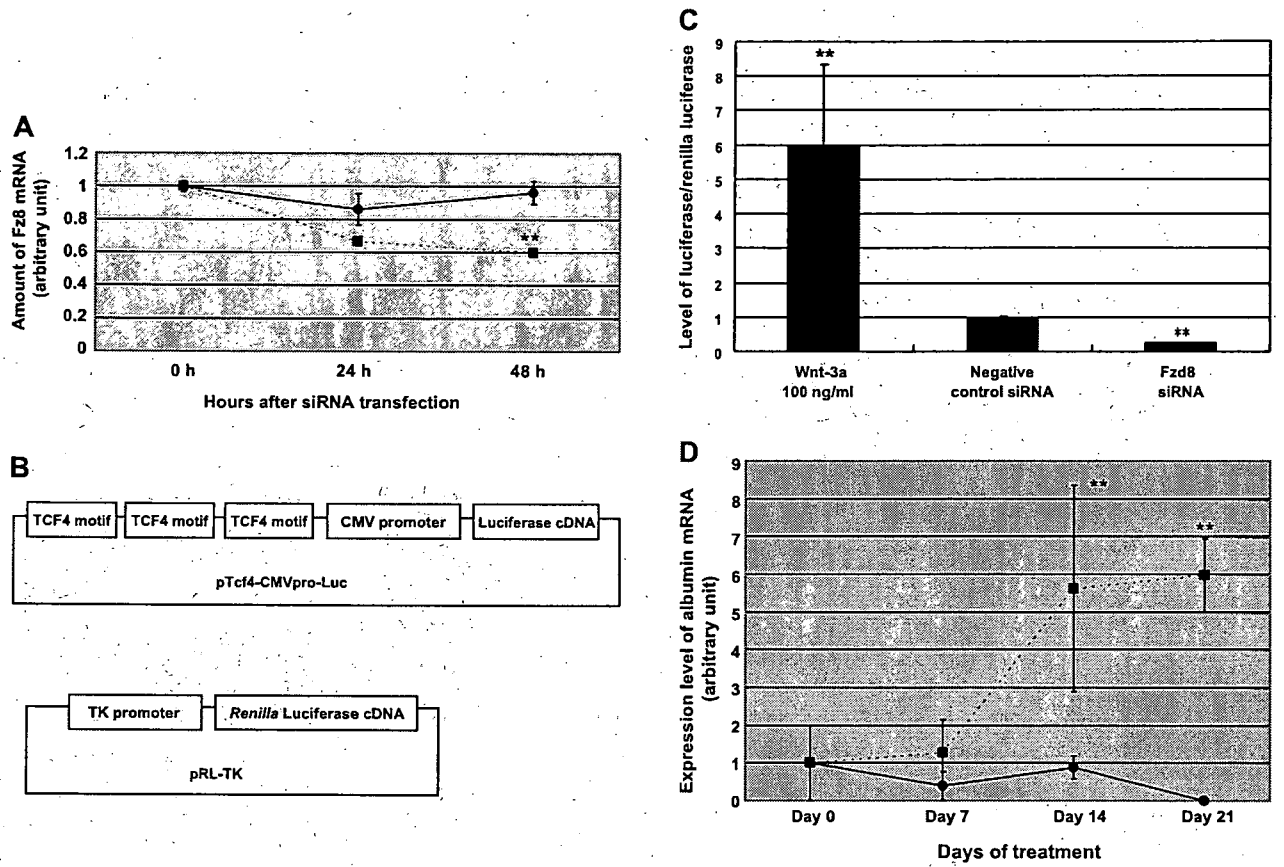

Fig. 4. Effect of Fz8-small interference RNA (siRNA) on hepatic differentiation of UCBTERT-21 cells. *A*: time course of Fz8 mRNA expression on transfection of Fz8-siRNA. The mRNA level of Fz8 was measured by real-time RT-PCR. The level of fzd8 was expressed as a ratio of that at 0 h. ●, negative control siRNA; ■, Fz8-siRNA. Data are expressed as means ± SE of 3 experiments. $^{**}P < 0.01$, compared with the negative control siRNA. *B*: construction of plasmids for the β-catenin-Tcf reporter gene assay. The plasmid contained 3 copies of the optimal Tcf motif upstream of the CMV promoter driving luciferase expression (Tcf4-CMVpro-Luc). A plasmid with the thymidine kinase promoter driving *Renilla* luciferase expression (pRL-TK) was used as an internal control. *C*: reduction of transactivational properties of β-catenin-Tcf4 in UCBTERT-21 cells transfected with fz8-siRNA. The activation level of β-catenin-Tcf4 was expressed as a ratio of that of the negative control siRNA. The level of luciferase activity was examined at 48 h after transfection of pTcf4-CMVpro-luc, pRL-TK, and Fz8-siRNA. The data are expressed as a ratio to *Renilla* luciferase activity. The data from the addition of 100 ng/ml Wnt-3a at 24 h after transfection served a positive control. Data are expressed as means ± SE of 6 experiments. $^{**}P < 0.001$, compared with negative control siRNA. *D*: expression of the albumin gene was induced by Fz8-siRNA transfection. The level of albumin, as evaluated by real-time RT-PCR, was expressed as a ratio of that on *day 0*. ●, negative control siRNA; ■, Fz8-siRNA. Data are expressed as means ± SE of 3 experiments. $^{**}P < 0.01$, compared with *day 0*. *Fig. 4 (Continues).*

development (26). In addition, nuclear β-catenin staining was not observed in hepatocytes from human autopsied tissues at gestational ages 10, 15, 16, 18, 22, and 35 wk (8). Recently, it has been reported that repression of Wnt/β-catenin signaling in the anterior endoderm is essential for development (32). Additional reports have shown a requirement for Wnt signaling after liver cells are formed and not at the time of endoderm specification to form the liver (3, 43). These reports support the results of the present study. In addition, a report that the combination of Wnt and other hepatic growth factors plays an important role in early liver development (13) is in agreement with the present study. It has been recently reported that mesodermal Wnt2b signaling positively regulates liver specification although the species used were different from the present study (34). Differences may arise as to how canonical Wnts can fulfill diverse functions in stem cell. The fact that stem cells from different locations interpret Wnt in different ways obviously reflects an activation of distinct genetic programs in response to the same signal. Although cyclin D1 and c-*myc* are direct target genes of β-catenin/Lef during cell cycle progression, recent studies revealed that proneural genes, neurogenins, are also targets of β-catenin/TCF/Lef during neurogenesis (11, 14). Thus the activation of specific sets of Wnt target genes is likely to be mediated by cell type-specific intrinsic properties. Besides the cell-intrinsic cues that influence the biological activity of Wnt in distinct stem and progenitor cell types, the same type of stem cell might respond in different ways to Wnts, depending on its extracellular microenvironment (17). In this model, Wnt signaling interacts with signaling pathways triggered by other cues and is involved in cross talk with other signals at several levels. Taken together, downregulation of the Wnt/β-catenin pathway plays an important role in the transdifferentiation of MSCs into hepatocytes in response to mesenchymal cell-specific intrinsic properties or cross talk between several cytokines.

In conclusion, we found that the downregulation of Wnt/β-catenin signals play an important role in hepatic differentiation of human UCBMSCs. During hepatic differentiation, Wnt/β-

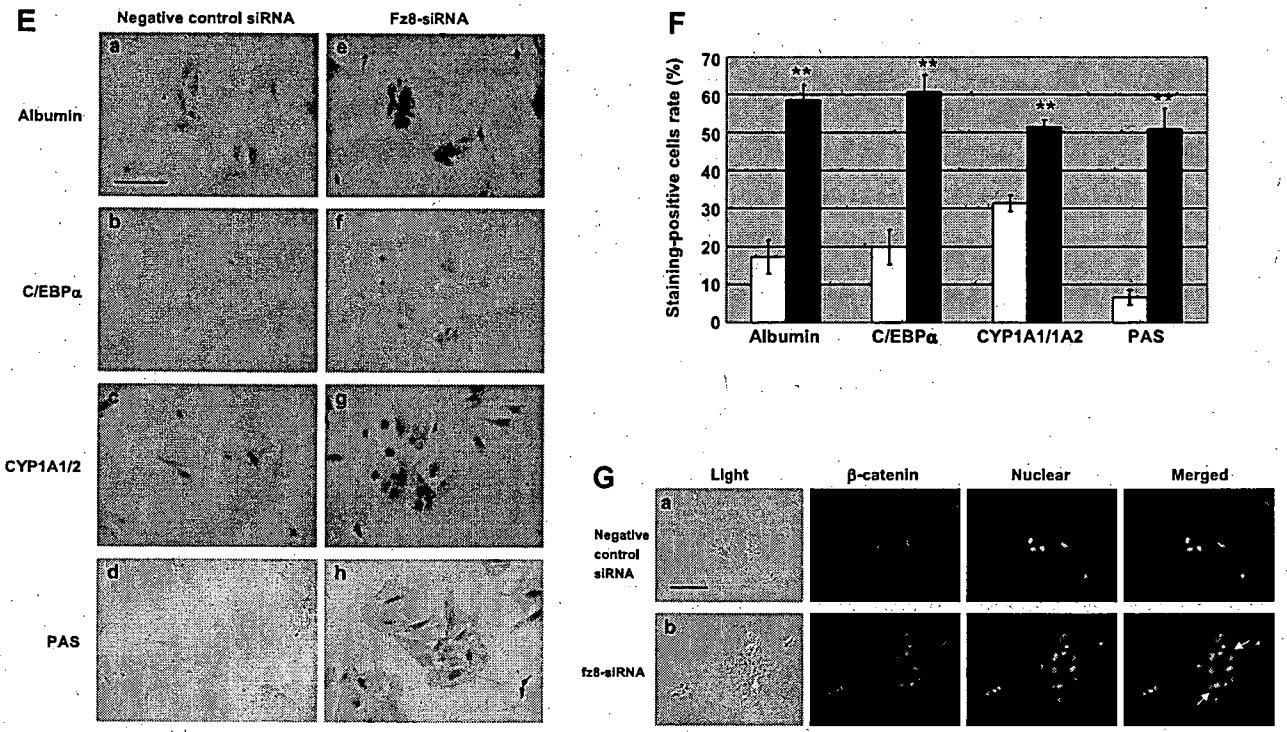

Fig. 4—*Continued.* *E*: induction of hepatocyte-specific proteins in UCBTERT-21 cells transfected with Fz8-siRNA on *day 21*. *a–d*, negative control siRNA; *e–h*, Fz8-siRNA. Cells were immunostained with anti-albumin (*a*, *e*), anti-C/EBPα (*b*, *f*), and anti-CYP1A1/1A2 (*c*, *g*) antibodies. Glycogen stored in cells was stained by PAS stain (*d*, *h*). Scale bar, 100 μm. *F*: efficiency of hepatic differentiation of UCBTERT-21 cells with fzd8-siRNA. Open bars, negative control siRNA; solid bars, Fz8-siRNA. Data are expressed as means ± SE of 6 experiments. $^{**}P < 0.001$ compared with negative control siRNA. *G*: localization of β-catenin in UCBTERT-21 cells transfected with Fz8-siRNA. *a*: Negative control siRNA on *day 21*. *b*: Fz8-siRNA on *day 21*. Light micrograph (Light), β-catenin staining (β-catenin), nuclear staining (Nuclear), and merged images of β-catenin and nuclear staining (Merged) are shown. SYTOX green was utilized for nuclear staining. β-Catenin was located in the cytoplasm (arrows) of several differentiated cells. Scale bar, 100 μm.

catenin signaling was downregulated. Conversely, suppression of the signaling stimulated the hepatic differentiation of UCBTERT-21 cells. These findings provide useful information on stem cell biology, which should contribute to the development of regenerative medicine for liver diseases.

REFERENCES

1. **Alison MR, Poulsom R, Jeffery R, Dhillon AP, Quaglia A, Jacob J, Novelli M, Prentice G, Williamson J, Wright NA.** Hepatocytes from non-hepatic adult stem cells. *Nature* 406: 257, 2000.
2. **Alvarez-Dolado M, Pardal R, Garcia-Verdugo JM, Fike JR, Lee HO, Pfeffer K, Lois C, Morrison SJ, Alvarez-Buylla A.** Fusion of bone marrow-derived cells with Purkinje neurons, cardiomyocytes and hepatocytes. *Nature* 425: 968–973, 2003.
3. **Apte U, Zeng G, Thompson MD, Muller P, Micsenyi A, Cieply B, Kaestner KH, Monga SPS.** β-Catenin is critical for early postnatal liver growth. *Am J Physiol Gastrointest Liver Physiol* 292: G1578–G1685, 2007.
4. **Cadigan KM, Liu YI.** Wnt signaling: complexity at the surface. *J Cell Sci* 119: 395–402, 2006.
5. **Cerec V, Glaise D, Garnier D, Morosan S, Turlin B, Drenou B, Gripon P, Kremsdorf D, Guguen-Gullouzo C, Corlu A.** Transdifferentiation of hepatocyte-like cells from the human hepatoma HepaRG cell line through bipotent progenitor. *Hepatology* 45: 957–967, 2007.
6. **Cerny J, Quesenberry PJ.** Chromatin remodeling and stem cell theory of relativity. *J Cell Physiol* 201: 1–16, 2004.
7. **D'Ippolito G, Schiller PC, Ricordi C, Roos BA, Howard GA.** Age-related osteogenic potential of mesenchymal stromal stem cells from human vertebral bone marrow. *J Bone Miner Res* 14: 1115–1122, 1999.
8. **Eberhart CG, Argani P.** Wnt signaling in human development: beta-catenin nuclear translocation in fetal lung, kidney, placenta, capillaries, adrenal, and cartilage. *Pediatr Dev Pathol* 4: 351–357, 2001.
9. **Fausto N.** Liver regeneration and repair: hepatocytes, prognostic cells, and stem cells. *Hepatology* 39: 1477–1487, 2004.
10. **Finley KR, Tennessen J, Shawlot W.** The mouse secreted frizzled-related protein 5 gene is expressed in the anterior visceral endoderm and foregut endoderm during early post-implantation development. *Genes Expr Patterns* 3: 681–684, 2003.
11. **Hirabayashi Y, Itoh Y, Tabata H, Nakajima K, Akiyama T, Masuyama N, Gotoh Y.** The Wnt/β-catenin pathway directs neuronal differentiation of cortical neural precursor cells. *Development* 131: 2791–2801, 2004.
12. **Huelsken J, Vogel R, Erdmann B, Cotsarelis G, Birchmeier W.** β-Catenin controls hair follicle morphogenesis and stem cell differentiation in the skin. *Cell* 105: 533–545, 2001.
13. **Hussain SZ, Sneddon T, Tan X, Micsenyi A, Michalopoulos GK, Monga SP.** Wnt impacts growth and differentiation in ex vivo liver development. *Exp Cell Res* 292: 157–169, 2004.
14. **Israsena N, Hu M, Fu W, Kan L, Kessler JA.** The presence of FGF2 signaling determines whether β-catenin exerts effects on proliferation or neural differentiation of neural stem cells. *Dev Biol* 268: 220–231, 2004.
15. **Jiang Y, Jahagirdar BN, Reinhardt RL, Schwartz RE, Keene CD, Ortiz-Gonzalez XR, Reyes M, Lenvik T, Lund T, Blackstad M, Du J, Aldrich S, Lisberg A, Low WC, Largaespada DA, Verfaillie CM.** Pluripotency of mesenchymal stem cells derived from adult marrow. *Nature* 418: 41–49, 2002.
16. **Jung J, Zheng M, Goldfarb M, Zaret KS.** Initiation of mammalian liver development from endoderm by fibroblast growth factors. *Science* 284: 1998–2003, 1999.
17. **Kleber M, Sommer L.** Wnt signaling and the regulation of stem cell function. *Curr Opin Cell Biol* 16: 681–687, 2004.
18. **Koh LP, Chao NJ.** Umbilical cord blood transplantation in adults using myeloablative and nonmyeloablative regimens. *Biol Blood Marrow Transplant* 10: 1–22, 2004.

19. **Kondo T.** Epigenetic alchemy for cell fate conversion. *Curr Opin Genet Develop* 16: 1–6, 2006.
20. **Korbling M, Katz RL, Khanna A, Ruifrok AC, Rondon G, Albitar M, Champlin RE, Estrov Z.** Hepatocytes and epithelial cells of donor origin in recipients of peripheral-blood stem cells. *N Engl J Med* 346: 738–746, 2002.
21. **Krause DS, Theise ND, Collector MI, Henegariu O, Hwang S, Gardner R, Neutzel S, Sharkis SJ.** Multi-organ, multi-lineage engraftment by a single bone marrow-derived stem cell. *Cell* 105: 369–377, 2001.
22. **Lagasse E, Connors H, Al-Dhalimy Reitsma M, Dohse M, Osborne L, Wang X, Finegold M, Weissman IL, Grompe M.** Purified hematopoietic stem cells can differentiate into hepatocytes in vivo. *Nat Med* 6: 1229–1234, 2000.
23. **Lakshmipathy U, Verfaillie C.** Stem cell plasticity. *Blood Rev* 19: 29–38, 2005.
24. **Lee KD, Kuo TK, Wang-Peng J, Chung YF, Lin CT, Chou SH, Chen JR, Chen YP, Lee OK.** In vitro hepatic differentiation of human mesenchymal stem cells. *Hepatology* 40: 1275–1284, 2004.
25. **Lee OK, Kuo TK, Chen WM, Lee KD, Hsieh SL, Chen TH.** Isolation of multipotent mesenchymal stem cells from umbilical cord blood. *Blood* 103: 1669–1675, 2004.
26. **Lemaigre F, Zaret KS.** Liver development update: new embryonic models, cell lineage control, and morphogenesis. *Curr Opin Genet Dev* 14: 582–590, 2004.
27. **Li X, Yost HJ, Virshup DM, Seling JM.** Protein phosphatase 2A and its B56 regulatory subunit inhibit Wnt signaling in Xenopus. *EMBO J* 20: 4122–4131, 2001.
28. **Lu FZ, Fujino M, Kitazawa Y, Uyama T, Hara Y, Funeshima N, Jiang JY, Umezawa A, Li XK.** Characterization and gene transfer in mesenchymal stem cells derived from human umbilical-cord blood. *J Lab Clin Med* 146: 271–278, 2005.
29. **Makino S, Fukuda K, Miyoshi S, Konishi F, Kodama H, Pan J, Sano M, Takahashi T, Hori S, Abe H, Umezawa A, Ogawa S.** Cardiomyocytes can be generated from marrow stromal cells in vitro. *J Clin Invest* 103: 697–705, 1999.
30. **Mayani H, Lansdorp PM.** Biology of human umbilical cord blood-derived hematopoietic stem/progenitor cells. *Stem Cells* 16: 153–165, 1998.
31. **Micsenyi A, Tan X, Sneddon T, Luo J, Michalopoulos GK, Monga SPS.** β-Catenin is temporally regulated during normal liver development. *Gastroenterology* 126: 1134–1146, 2004.
32. **McLin VA, Rankin SA, Zorn A.** Repression of Wnt/β-catenin signaling in the anterior endoderm is essential for liver and pancreas development. *Development* 134: 2207–217, 2007.
33. **Muroyama Y, Fujihara M, Ikeya M, Kondoh H, Takada S.** Wnt signaling plays an essential role in neuronal specification of the dorsal spinal cord. *Genes Dev* 16: 548–553, 2002.
34. **Ober EA, Verkade H, Field HA, Satinier DY.** Mesodermal Wnt2b signalling positively regulates liver specification. *Nature* 442: 688–691, 2006.
35. **Pilcher KE, Krieg PA.** Expression of the Wnt inhibitor, sFRP5, in the gut endoderm of Xenopus. *Gene Expr Patterns* 2: 369–372, 2002.
36. **Ratcliffe MJ, Itoh K, Sokol SY.** A positive role for the PP2A catalytic subunit in Wnt signal transduction. *J Biol Chem* 175: 35680–35683, 2000.
37. **Reya T, Duncan AW, Alles L, Domen J, Scherer DC, Willert K, Hintz L, Nusse R, Weissman IL.** A role for Wnt signalling in self-renewal of haematopoietic stem cells. *Nature* 423: 409–414, 2003.
38. **Roose J, Huls G, Beest von M, Moerer P, van der Horn K, Goldschmeding R, Logtenberg T, Clevers H.** Synergy between tumor suppressor APC and the b-catenin-Tcf4 target Tcf1. *Science* 285: 1923–1926, 1999.
39. **Sato N, Meijer L, Skaltsounis L, Greengard P, Brivanlou AH.** Maintenance of pluripotency in human and mouse embryonic stem cells through activation of Wnt signaling by a pharmacological GSK-3-specific inhibitor. *Nat Med* 10: 55–63, 2004.
40. **Schmidt C, Bladt F, Goedecke S, Brinkmann V, Zschiesche W, Sharpe M, Gherardi E, Birchmeier C.** Scatter factor/hepatocyte growth factor is essential for liver development. *Nature* 373: 699–702, 1995.
41. **Schwartz RE, Reyes M, Koodie L, Jiang Y, Blackstad M, Lund T, Lenvik T, Johnson S, Hu WS, Verfaillie CM.** Multipotent adult progenitor cells from bone marrow differentiate into functional hepatocyte-like cells. *J Clin Invest* 109: 1291–1302, 2002.
42. **Shiota G, Okano J, Kawasaki H, Kawamoto T, Nakamura T.** Serum hepatocyte growth factor levels in liver diseases: clinical implications. *Hepatology* 21: 106–112, 1995.
43. **Suksawaeng S, Lin CM, Jiang TX, Hughes MW, Widelitz RB, Chuong CM.** Morphogenesis of chicken liver: identification of localized growth zones and the role of β-catenin/Wnt in size regulation. *Development* 266: 109–122, 2004.
44. **Tago K, Nakamura T, Nishita M, Hyodo J, Nagai S, Murata Y, Adachi S, Ohwada S, Morishita Y, Shibuya H, Akiyama T.** Inhibition of Wnt signaling by ICAT, a novel β-catenin-interacting protein. *Genes Dev* 14: 1741–1749, 2000.
45. **Tanabe Y, Tajima F, Nakamura Y, Shibasaki E, Wakejima M, Shimomura T, Murai R, Murawaki Y, Hashiguchi K, Kanbe T, Saeki T, Ichiba M, Yoshida Y, Mitsunari M, Yoshida S, Miake J, Yamamoto Y, Nagata N, Harada T, Kurimasa A, Hisatome I, Terakawa N, Murawaki Y, Shiota G.** Analyses of clarify rich fractions in hepatic progenitor cells from human umbilical cord blood and cell fusion. *Biochem Biophys Res Commun* 324: 711–718, 2004.
46. **Terai M, Uyama T, Sugiki T, Li XK, Umezawa A, Kiyono T.** Immortalization of human fetal cells: the life span of umbilical cord blood-derived cells can be prolonged without manipulating $p16^{INK4a}$/RB braking pathway. *Mol Biol Cell* 16: 1491–1499, 2005.
47. **Theise ND, Nimmmakakalu M, Gardner R, Illei PB, Morgan G, Teperman L, Henegariu O, Krause DS.** Liver from bone marrow in human. *Hepatology* 31: 235–240, 2000.
48. **Zaret KS.** Genetic control of hepatocyte differentiation. In: *The Liver* (3rd ed.), edited by Arias IM, Boyer JL, Fausto N, Jakoby WB, Schachter D, and Shafritz DA. New York: Raven, 1994, p. 53–68.

Available online at www.sciencedirect.com
ScienceDirect
ELSEVIER
Biochemical and Biophysical Research Communications 364 (2007) 838–843
BBRC
www.elsevier.com/locate/ybbrc

Preferential localization of SSEA-4 in interfaces between blastomeres of mouse preimplantaion embryos

Ban Sato [a,e], Yohko U. Katagiri [a,d,*], Kenji Miyado [b], Hidenori Akutsu [b], Yoshitaka Miyagawa [a], Yasuomi Horiuchi [a], Hideki Nakajima [a], Hajime Okita [a,d], Akihiro Umezawa [b], Jun-ichi Hata [a], Junichiro Fujimoto [c,d,1], Kiyotaka Toshimori [e], Nobutaka Kiyokawa [a,d]

[a] *Department of Developmental Biology, National Research Institute for Child Health and Development, 2-10-1 Okura, Setagaya-ku, Tokyo 157-8535, Japan*
[b] *Department of Reproductive Biology, National Research Institute for Child Health and Development, 2-10-1 Okura, Setagaya-ku, Tokyo 157-8535, Japan*
[c] *National Research Institute for Child Health and Development, 2-10-1 Okura, Setagaya-ku, Tokyo 157-8535, Japan*
[d] *Core Research for Evolutional Science and Technology (CREST) of Japan Science and Technology Corporation (JST), Japan*
[e] *Department of Anatomy and Developmental Biology, Graduate School of Medicine, Chiba University, Chiba 260-8670, Japan*

Received 11 October 2007
Available online 26 October 2007

Abstract

The monoclonal antibody 6E2 raised against the embryonal carcinoma cell line NCR-G3 had been shown to also react with human germ cells. Thin-layer chromatography (TLC) immunostaining revealed that 6E2 specifically reacts with sialosylglobopentaosylceramide (sialylGb5), which carries an epitope of stage-specific embryonic antigen-4 (SSEA-4), known as an important cell surface marker of embryogenesis. The immunostaining of mouse preimplantation embryos without fixation showed that the binding of 6E2 caused the clustering and consequent accumulation of sialylGb5 at the interface between blastomeres. These results suggest that SSEA-4 actively moves on the cell surface and readily accumulates between blastomeres after binding of 6E2.

Keywords: SialylGb5; SSEA-4; Embryonic stem cells; Embryonal carcinoma cells; Preimplantation embryo; Immunostaining

Embryonal carcinoma (EC) cells isolated from teratocarcinomas have been shown to possess pluri- or multipotency in both mouse and human systems [1–3]. In mice, certain EC cells as well as embryonic stem (ES) cells have been considered to be developmentally equivalent to the inner cell mass of blastocysts [1]. These EC cells are useful for clarifying the molecular characteristics of early embryonic cells and thus many efforts have been made to establish EC cell lines and monoclonal antibodies (Mabs) that detect differentiation-related molecules on EC cells. As a consequence, a number of stage-specific markers for embryogenesis have been identified. Notably, it is important that this molecular information is adapted to research on ES cells or mouse preimplantation embryos. Stage-specific embryonic antigen (SSEA) -1, -3, and -4, as well as tumor rejection antigen (TRA) -1-60 and -1-81 [4], have been used as stage-specific markers for embryogenesis, though their functional significance in early development remains unclear. Interestingly, however, most of these antigens are carbohydrates themselves or closely related to the carbohydrates carried on glycosphingolipids (GSLs) and glycoproteins [5].

6E2 is a Mab established by immunizing with NCR-G3 cells, a previously established multipotent human EC cell

* Corresponding author. Address: Department of Developmental Biology, National Research Institute for Child Health and Development, 2-10-1 Okura, Setagaya-ku, Tokyo 157-8535, Japan. Fax: +81 3 3417 2496.
E-mail address: kata@nch.go.jp (Y.U. Katagiri).
[1] Vice General Director.

0006-291X/$ - see front matter © 2007 Elsevier Inc. All rights reserved.
doi:10.1016/j.bbrc.2007.10.093

line capable of differentiating into trophoblastic cell lineages other than somatic cells [3]. It has been revealed that 6E2 reacts with not only human ECs, including NCR-G2 and 3 cells, but also other germ cell tumors, as well as normal human germ cells such as spermatogonia and oocytes [6]. Although a previous study reported that 6E2 immunoprecipitates a cell surface protein having a molecular weight of approximately 80 kDa from ^{125}I-labeled NCR-G3 cells, the specific antigen recognized by 6E2 still remains unknown. To characterize the antigen specificity of 6E2, we examined the reactivity of the Mab with other cell lines using several distinct methods. In this paper, we present evidence that 6E2 recognizes SSEA-4 carried by sialylGb5. Using 6E2, we determined the localization of SSEA-4 in "living" mouse preimplantation embryos and observed its preferential localization in interface between blastomeres.

Materials and methods

Cells, antibodies, and animals. The human renal carcinoma cell line ACHN was purchased from American Type Culture Collection. The African green monkey kidney cell line Vero was a gift from Dr. T. Takeda of Department of Infectious Diseases Research, National Children's Medical Research Center, Tokyo, Japan. Cells were maintained in Dulbecco's modified Eagle's minimum essential medium (DMEM) (Sigma Chem., St. Louis, MO) supplemented with 10% fetal bovine serum (FBS) (JRH Bioscience, Lenexa, KS). The human EC cell line NCR-G2 [3] was cultured in a 1:1 mixture of DMEM and Ham's F12 medium (DMEM/F12) (Invitrogen Gibco, Carlsbad, CA) supplemented with 10% FBS(JRH Bioscience), non-essential amino acid solution (NEAA) (Invitrogen Gibco), and Insulin-Transferin-Sodium Selenite media (Invitrogen Gibco). The cynomolgus monkey ES cell line CMK-6 [7] were provided by Dr. Yasushi Kondo of Mitsubishi Tanabe Pharma Corporation. ES cells were grown on mouse embryonic fibroblast feeder cells that were inactivated by gamma-irradiation in DMEM/F12 supplemented with 20% Knockout™ Serum Replacement, 2 mM Glutamax-I, 1% NEAA, 50 units/ml penicillin, 50 μg/ml streptomycin, 0.1 mM 2-mercaptoethanol, 1% sodium pyruvate, and 5 ng/ml bFGF (all from Invitrogen GIBCO). The cultures were performed at 37 °C in a 5% CO_2 incubator. The human venous blood from a healthy consenting volunteer was drawn in a heparin-coated syringe. The blood was spun at 3000 rpm for 15 min and human red blood cells (hRBCs) were washed three times in phosphate buffered saline (PBS).

The conjugation of affinity-purified 6E2 (mouse IgG_3, κ) [6] to the fluorescence reagent was performed with an Alexa Fluor® 488 monoclonal antibody labeling kit (Molecular Probes, Eugene, OR.) according to the manufacturer's instructions. The anti-SSEA-4 Mabs used in this study were Raft.2 [8] and MC813-70 (R&D Systems, Inc Minneapolis, MN). Alexa Fluor® 488 goat anti-mouse IgG and Streptavidin Alexa Fluor® 568 were purchased from Molecular probes.

BDF_1 mice were purchased from Clea Japan (Tokyo, Japan).

TLC immunostaining of GSLs. TLC immunostaining of GSLs from cultured cells and hRBCs was performed as previously described [9]. Reference GSLs were purchased from Matlayer, Inc. (Pleasant Gap, PA). SialylGb5 was purified from ACHN cells by preparative TLC. Purified GM1 b was kindly provided by Dr. Nakamura of RIKEN, Saitama, Japan [10].

Flow cytometry. Cells were harvested and incubated with a primary antibody (1 μg/ml) for 1 h on ice, followed by treatment with fluorescein isothiocyanate-conjugated goat anti-mouse immunoglobulins (Jackson Immunoresearch Laboratories, Inc., West Grove, PA) at a dilution of 1:50 and analyzed with an EPICS-XL flow cytometer (Beckman Coulter, Inc, Miami, FL).

Dot blot analysis. Purified sialylGb5 was serially diluted (0.1–60 ng) and vacuum blotted onto a PVDF membrane by using a 96-well format dot blot apparatus (Bio-Rad Laboratories, Richmond, CA). The membrane was immunostained with the Mab 6E2 or MC813-70 (0.5 μg/ml) according to a previously described procedure [9]. The antibodies that bound to the membranes were visualized with ECL-plus Western Blotting Detection Reagents (GE Healthcare UK Ltd, Buckinghamshire, UK) and scanned with a LAS-1000 luminescent imaging analyzer (Fujifilm, Tokyo, Japan). Scanned images were analyzed using the software Image Gauge with which the LAS-1000 was equipped.

Indirect immunostaining of cynomolgus monkey ES cells. Cells were grown on a glass-bottomed dish (IWAKI) for 3 days and then these cells were fixed for 30 min with 4% paraformaldehyde in PBS and permeabilized with 0.2% Triton X-200 in PBS for 20 min. Subsequently, the cells were washed three times with PBS for 5 min and blocked with 5% normal goat serum in PBS for 30 min. The fixed cells were incubated with anti-SSEA-4 antibodies or isotype-matched mouse IgG at a dilution of 1:300 for 2 h, followed by incubation with Alexa Fluor® 488-conjugated goat anti-mouse IgG at a dilution of 1:300 for 30 min. DAPI was used for counter staining of nuclei.

Immunostaining of mouse preimplantation embryos. Mouse preimplantation embryos were collected from superovulated mice. Seven-week-old BDF1 female mice were induced to superovulate with intraperitoneal injections of pregnant mare's serum gonadotropin (ASKA Pharmaceutical co., Ltd., Tokyo, Japan) (5 IU) and human chorionic gonadotropin (hCG) (ASKA Pharmaceutical co) (5 IU) 48 h apart and mated with individual BDF1 male mice after the hCG injection. The 2-cell, the 8-cell, and the morula stage embryos were flushed out from oviducts at 36, 60, and 72 h after the hCG injection, respectively. Animals were treated according to the institutional animal care and use guidelines of National Research Institute for Child Health and Development.

Embryos immediately after being collected and those prefixed with 2% paraformaldehyde in Hepes buffered saline were incubated in 30 μl drops of M16 medium containing 0.45 μg of Alexa Fluor® 488-conjugated 6E2 for 1 h or biotinylated MC813-70 for 1 h, treated with streptavidin Alexa Fluor® 568 diluted 1:300, and then they were washed three times in 30 μl drops of M16 medium. All staining steps were carried out at 37 °C in a CO_2 incubator for fresh embryos and at 4 °C for fixed embryos. The stained embryos were placed in drop of a M16 medium on glass-bottomed dishes (IWAKI, Tokyo, Japan), and were observed with a LSM510 Zeiss Confocal laser-scanning microscope (Carl Zeiss, Thornwood, NY) to obtain a field of view of the embryo only with a 40× objective lens.

Results and discussion

6E2 specifically binds to sialylGb5

In order to examine whether the 80 kDa membrane protein is recognized by 6E2, we performed a Western analysis of the cell lysates or their immunoprecipitates with 6E2. Since no significant signal was detected on the blot (data not shown), we examined TLC immunostaining of GSLs extracted from several 6E2-positive cell lines. ACHN cells showed the expression of comparable amounts of Gb3, Gb4, Gb5, and sialylGb5, whereas Vero cells and NCR-G2 cells expressed predominantly Gb3 (Fig. 1A). TLC immunostaining analysis revealed that 6E2 binds to a major slow-migrating GSL extracted from these three cell lines. The slow-migrating GSL was identified as sialylGb5, defined by the Mab Raft.2. We observed that 6E2 bound to sialylGb5 (LKE-antigen) of hRBCs [13] (Fig. 1B). Finally, we examined the reactivity of 6E2 with purified GSLs and found that the Mab reacts with purified sialylGb5, but not purified GM1 b (Fig. 1C). These results indicate that 6E2 specifically binds to sialylGb5 and thus is an anti-SSEA-4

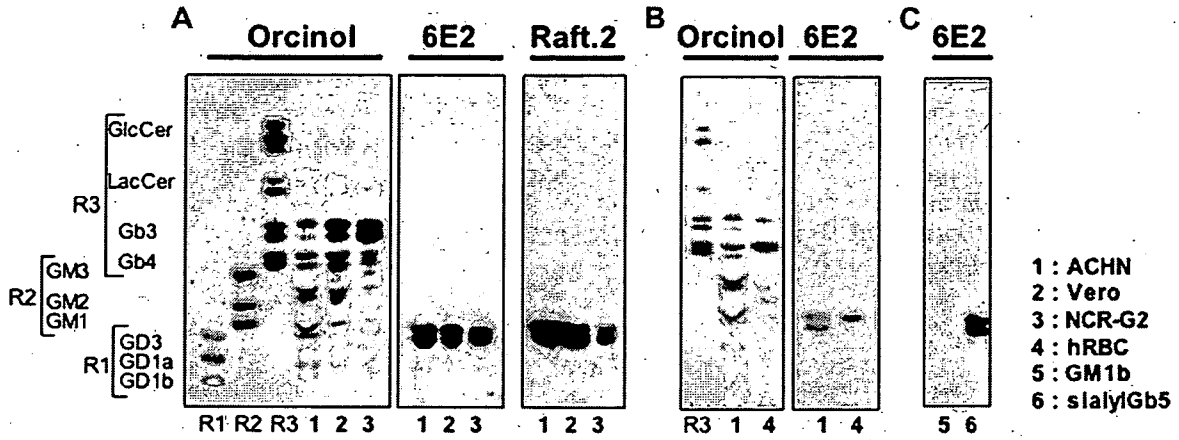

Fig. 1. TLC immunostaining of GSLs prepared from cultured cells and hRBCs. GSLs extracted from cultured cells and hRBCs or purified GSLs were separated by TLC in a solvent system of chloroform/methanol/water containing 0.2% $CaCl_2$ (5:4:1, v/v/v). Plates were chemically stained with orcinol-sulfurnic acid or were immunostained with 6E2 and Raft.2. Lane 1, ACHN; Lane 2, Vero; Lane 3, NCR-G2; Lane 4, hRBCs; Lane 5, GM1b; Lane 6, sialylGb5. Reference markers used were disialosyl gangliosides of GD3, GD1a, and GD1b (R1), monosialosyl gangliosides of GM3, GM2, and GM1 (R2), and neutral GSLs of GlcCer, LacCer, Gb3, and Gb4 (R3). The nomenclature for GSLs follows the recommendations [11] of the IUB, and the ganglioside nomenclature of Svennerholm [12] was used.

Mab. The 80 kDa protein might be associated with sialylGb5 in NCR-G3 cells and thus co-immunoprecipitated by 6E2.

Comparison of reactivity to sialyl Gb5 between 6E2 and MC813-70

MC813-70 established by immunizing with human EC cell lines has been most widely used as an anti-SSEA-4 antibody (mouse IgG_3, κ) [14]. Therefore we compared the reactivities of the Mabs 6E2 and MC813-70 by flow cytometry and dot-blot immunostaining. The fluorescence intensity obtained with 6E2 was stronger than that with MC813-70 in each cell line and hRBCs (Fig. 2A). A recent flow cytometric study showed that MC813-70 strongly stains hRBCs, but other anti-sialyGb5 Mabs do not [15]. However, our data indicate that 6E2 is more reactive than MC813-70. Next we compared the reactivity of the two

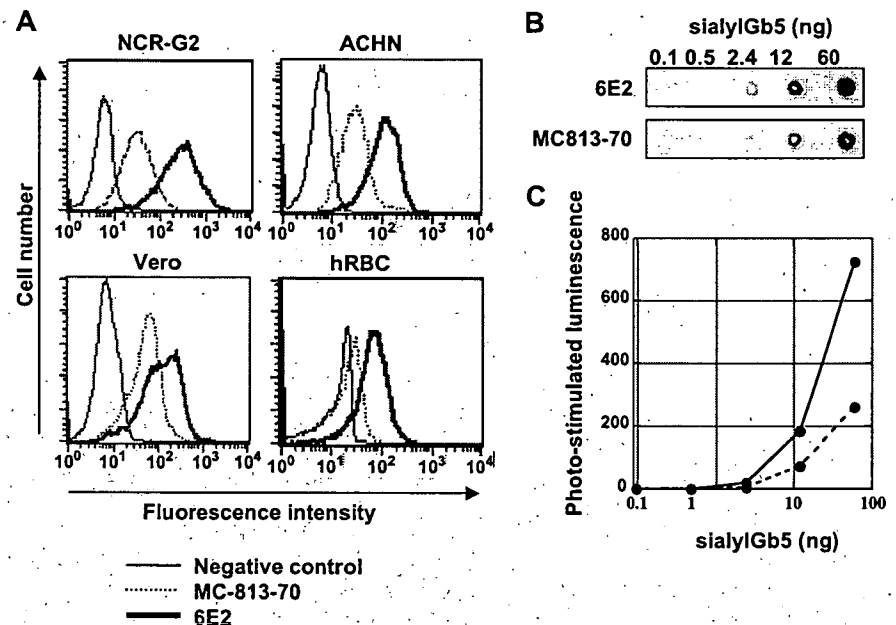

Fig. 2. Reactivity of 6E2 and MC813-70 with sialylGb5. (A) Flow cytometric analysis of SSEA-4-positive cells with 6E2. NCR-G2 cells, ACHN cells, Vero cells, and hRBCs were stained with 6E2 (bold line) or MC813-70 (dotted line) and with a FITC-conjugated secondary antibody and analyzed by flow cytometry. (B) An image of the dot-blot immunostaining of sialylGb5 obtained with a LAS-1000 luminescent imaging analyzer. (C) Measurement of antibodies bound (6E2: solid line, MC813-70: broken line).

Mabs with that of sialylGb5 by dot-blot immunostaining. Serially diluted sialylGb5 was dot-blotted onto a PVDF membrane, and the membrane was immunostained with the two Mabs. Both 6E2 and MC813-70 bound to more than 12 ng of sialylGb5, but the signals induced by 6E2 were stronger than those induced by MC813-70 (Fig. 2B,C). Thus, in addition to the flow cytometric analysis, the reactivity of 6E2 with sialylGb5 was stronger than that of MC813-70 by dot-blot immunostaining.

SSEA-4 Immunostaining of cynomolgus monkey ES cells

To confirm whether Mab 6E2 reacts with SSEA-4 on monkey ES cells, we performed an indirect immunofluorescence staining of cynomolgus monkey ES cells with Mab 6E2 and MC813-70. Mab 6E2 reacted with monkey ES cells (Fig. 3A) as well as MC-813-70 did (Fig. 3B). No difference in staining patterns of SSEA-4 between the two Mabs was observed. Mab 6E2 certainly stained SSEA-4 on monkey ES cells.

SSEA-4 immunostaining of "living" mouse preimplantation embryos without fixation

During early embryogenesis in mice, SSEA-4 had been reported to be expressed in fertilized eggs with levels gradually increasing to the morula stage and then decreasing [5]. Thus we examined the expression and distribution of SSEA-4 in preimplantation mouse embryos by immunostaining with both 6E2 and MC813-70. Both Mabs evenly stained the whole surface membranes of fixed mouse embryos, and no difference in staining pattern between the two was observed (data not shown). In order to perform a time-course of SSEA-4 distribution in a viable state, we performed immunostaining of preimplantation embryos without fixation.

3D-images of the 6E2 staining pattern obtained by confocal laser scanning microscopic observation clearly showed the localization of SSEA-4 on mouse preimplantation embryos. Two-cell embryos showed patches of SSEA-4 over the whole surface membrane with some accumulation at the interface between blastomeres (Fig. 4A). In 8-cell embryos, the amount accumulated at interfaces was further increased, as if planer membranes separate each blastomere, and some large patches were internalized but others were left on the surface membranes (Fig. 4B). The amount of SSEA-4 concentrated at the interfaces in morula was not as significant as in 8-cell embryos but still clearly observed and some patches were internalized (Fig. 4C).

2D-images of embryos stained with 6E2 showed a marked accumulation of SSEA-4 at the interfaces between blastomeres (Fig. 4D–F). These results suggest that sialylGb5 actively moves during development and tends to accumulate where blastomeres come into contact with each other.

Interestingly, however, the staining pattern of SSEA-4 using MC813-70 was different from that using 6E2. MC813-70 evenly stained the surface and the interface between blastomeres of 2-cell embryos with patches (Fig. 4G), and the amount of SSEA-4 at interfaces was not significant (Fig. 4J). In 8-cell embryos, there were patches of SSEA-4 in the central area of the outer surface of each blastomere (Fig. 4H, indicated by arrows), but the 2D-image showed that clustering also occurred at surfaces facing blastocoels (Fig. 4K, indicated by arrowheads). In morula embryos, SSEA-4 was distributed on the surface in patches and was enriched at the boundaries between blastomeres on the outer surface (Fig. 4I,L).

It remains unclear why the pattern of staining of mouse preimplantation embryos differs between 6E2 and MC813-70. The composition of fatty acids in GSLs influences the binding of antibodies [16,17] or bacterial toxins [18]. SialylGb5 recognized by the two MAbs might differ in composition of fatty acids, resulting in different immunostaining patterns. It was reported that the clustering of sialylGb5 by a Mab induces the activation of sialylGb5-associated kinases in raft microdomains of human mammary carcinoma cells, leading to downstream signaling [19,20]. The clustering of sialyGb5 by 6E2 on preimplantation mouse embryos may also induce the activation of some kinases, followed by downstream signaling. Recently, Comisky et al. suggested that lipid rafts and their associated molecules are spatiotemporally positioned to play a critical role in preimplantation developmental events [21]. The patches or clusters of sialylGb5 shown in our study suggest the presence of lipid rafts containing sialylGb5 on mouse embryos.

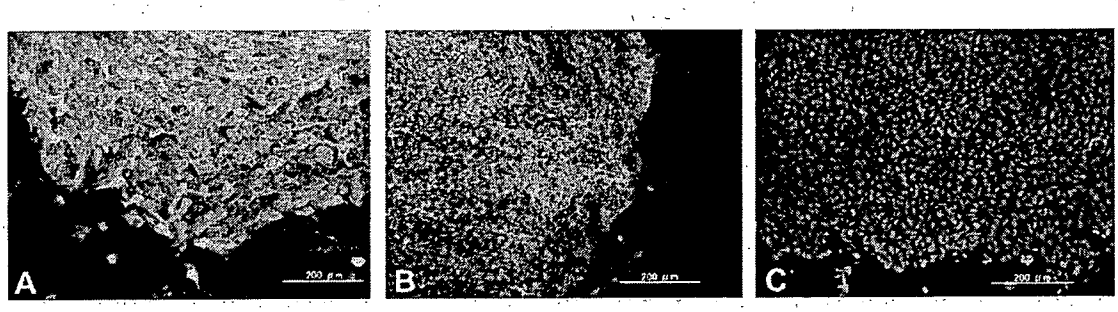

Fig. 3. Indirect immunostaining of cynomolgus monkey ES cell line CMK-6 with 6E2 and MC813-70. The CMK-6 cells were stained with 6E2 (A), MC813-70 (B), or isotype-matched mouse IgG (C), and visualized with secondary antibodies (green), followed by counterstaining of nuclei with DAPI (blue). Scale bars = 200 μm.

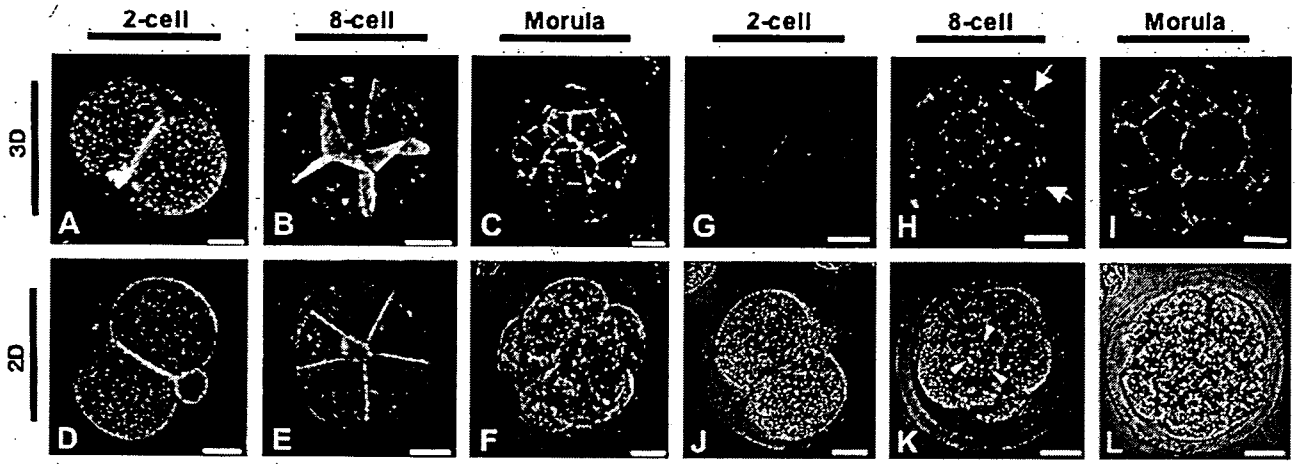

Fig. 4. Immunostaining of SSEA-4 on mouse preimplantation embryos with 6E2 and MC813-70. The embryos at the 2-cell (A, D, G, J), the 8-cell (B, E, H, K), and the morula (C, F, I, L) stages were stained with 6E2 (green) or MC813-70 (red). The panels designated 3D (A, B, C, G, H, I) are three-dimensional images reconstructed by stacking optical slice images using LSM software and the panels designated 2D (D, E, F, J, K, L) are an overlay of a fluorescent image and a differential interference contrast micrograph. Scale bars = 20 μm.

6E2 has high affinity for sialylGb5 and can be effectively conjugated with fluorescence reagents, leading to excellent staining of SSEA-4 in the surface membrane of "living" mouse preimplantation embryos. 6E2 should be of use for research into lipid rafts in early development and of great advantage for the characterization of ES cells and EC cells.

Acknowledgments

We thank S. Yamauchi for her excellent secretarial work. This work was supported in part by grants from CREST of JST and the 3rd. term comprehensive 10-year-strategy for cancer control, Research on Children and Families, Research on Human Genome Tailor made and Research on Publicly Essential Drugs and Medical Devices, Health and Labour Sciences Research Grants from the Ministry of Health, Labour and Welfare of Japan and a grant from The Japan Leukemia Research Field.

References

[1] B. Mintz, K. Illmensee, Normal genetically mosaic mice produced from malignant teratocarcinoma cells, Proc. Natl. Acad. Sci. USA 72 (1975) 3585–3589.
[2] P.W. Andrews, I. Damjanov, D. Simon, G.S. Banting, C. Carlin, N.C. Dracopoli, J. Fogh, Pluripotent embryonal carcinoma clones derived from the human teratocarcinoma cell line Tera-2. Differentiation in vivo and in vitro, Lab Invest. 50 (1984) 147–162.
[3] J.F. Jun-ichi Hata, Eizaburo Ishii, Akihiro Umezawa, Yasuo Kokai, Yoshie Matsubayashi, Hiroshi Abe, Satoru Kusakari, Haruto Kikuchi, Taketo Yamada, Tatsuya Maruyama, Differntiation of human germ cell tumor cells *in vivo* and *in vitro*, Acta Histochem. Cytochem. 25 (1992) 563–576.
[4] J.S. Draper, C. Pigott, J.A. Thomson, P.W. Andrews, Surface antigens of human embryonic stem cells: changes upon differentiation in culture, J. Anat. 200 (2002) 249–258.
[5] T. Muramatsu, H. Muramatsu, Carbohydrate antigens expressed on stem cells and early embryonic cells, Glycoconj. J. 21 (2004) 41–45.
[6] T. Nakano, A. Umezawa, H. Abe, N. Suzuki, T. Yamada, S. Nozawa, J. Hata, A monoclonal antibody that specifically reacts with human embryonal carcinomas, spermatogonia and oocytes is able to induce human EC cell death, Differentiation 58 (1995) 233–240.
[7] M. Yamamoto, N. Tase, T. Okuno, Y. Kondo, S. Akiba, N. Shimozawa, K. Terao, Monitoring of gene expression in differentiation of embryoid bodies from cynomolgus monkey embryonic stem cells in the presence of bisphenol A, J. Toxicol. Sci. 32 (2007) 301–310.
[8] Y.U. Katagiri, K. Ohmi, C. Katagiri, T. Sekino, H. Nakajima, T. Ebata, N. Kiyokawa, J. Fujimoto, Prominent immunogenicity of monosialosyl galactosylgloboside, carrying a stage-specific embryonic antigen-4 (SSEA-4) epitope in the ACHN human renal tubular cell line-a simple method for producing monoclonal antibodies against detergent-insoluble microdomains/raft, Glycoconj. J. 18 (2001) 347–353.
[9] Y.U. Katagiri, N. Kiyokawa, K. Nakamura, H. Takenouchi, T. Taguchi, H. Okita, A. Umezawa, J. Fujimoto, Laminin binding protein, 34/67 laminin receptor, carries stage-specific embryonic antigen-4 epitope defined by monoclonal antibody Raft.2, Biochem. Biophys. Res. Commun. 332 (2005) 1004–1011.
[10] K. Nakamura, Y. Hashimoto, M. Suzuki, A. Suzuki, T. Yamakawa, Characterization of GM1b in mouse spleen, J. Biochem. (Tokyo) 96 (1984) 949–957.
[11] The nomenclature of lipids (recommendations 1976). IUPAC-IUB Commission on Biochemical Nomenclature, J. Lipid. Res. 19 (1978) 114–128.
[12] L. Svennerholm, Designation and schematic structure of gangliosides and allied glycosphingolipids, Prog. Brain Res. 101 (1994) XI–XIV.
[13] L.L. Cooling, K. Kelly, Inverse expression of P(k) and Luke blood group antigens on human RBCs, Transfusion 41 (2001) 898–907.
[14] L.H. Shevinsky, B.B. Knowles, I. Damjanov, D. Solter, Monoclonal antibody to murine embryos defines a stage-specific embryonic antigen expressed on mouse embryos and human teratocarcinoma cells, Cell 30 (1982) 697–705.
[15] L. Cooling, D. Hwang, Monoclonal antibody B2, a marker of neuroendocrine sympathoadrenal precursors, recognizes the Luke (LKE) antigen, Transfusion 45 (2005) 709–716.
[16] K. Iwabuchi, I. Nagaoka, Lactosylceramide-enriched glycosphingolipid signaling domain mediates superoxide generation from human neutrophils, Blood 100 (2002) 1454–1464.
[17] K. Iwabuchi, Y. Zhang, K. Handa, D.A. Withers, P. Sinay, S. Hakomori, Reconstitution of membranes simulating "glycosignaling

domain" and their susceptibility to lyso-GM3, J. Biol. Chem. 275 (2000) 15174–15181.
[18] A. Kiarash, B. Boyd, C.A. Lingwood, Glycosphingolipid receptor function is modified by fatty acid content. Verotoxin 1 and verotoxin 2c preferentially recognize different globotriaosyl ceramide fatty acid homologues, J. Biol. Chem. 269 (1994) 11138–11146.
[19] W.F. Steelant, Y. Kawakami, A. Ito, K. Handa, E.A. Bruyneel, M. Mareel, S. Hakomori, Monosialyl-Gb5 organized with cSrc and FAK in GEM of human breast carcinoma MCF-7 cells defines their invasive properties, FEBS Lett. 531 (2002) 93–98.
[20] S. Van Slambrouck, W.F. Steelant, Clustering of monosialyl-Gb5 initiates downstream signalling events leading to invasion of MCF-7 breast cancer cells, Biochem. J. 401 (2007) 689–699.
[21] M. Comiskey, C.M. Warner, Spatio-temporal localization of membrane lipid rafts in mouse oocytes and cleaving preimplantation embryos, Dev. Biol. 303 (2007) 727–739.

FEBS Letters 581 (2007) 4685–4690

Eye-open at birth phenotype with reduced keratinocyte motility in LGR4 null mice

Shigeki Kato[a,1], Yasuaki Mohri[a], Tsuyoshi Matsuo[a], Eisaku Ogawa[b], Akihiro Umezawa[c], Ryuhei Okuyama[b], Katsuhiko Nishimori[a,*]

[a] *Laboratory of Molecular Biology, Graduate School of Agricultural Science, Tohoku University, 1-1 Tsutsumidori-Amamiyamachi, Aoba-ku, Sendai 981-8555, Japan*
[b] *Department of Dermatology, Tohoku University Graduate School of Medicine, 2-1 Seiryo-machi, Aoba-ku, Sendai 980-8574, Japan*
[c] *National Research Institute for Child Health and Development, 2-10-1, Okura, Setagaya-ku, Tokyo 157-8535, Japan*

Received 30 July 2007; accepted 27 August 2007

Available online 4 September 2007

Edited by Ned Mantei

Abstract **We observed a consistent eye-open at birth (EOB) phenotype in mouse pups homozygous for a leucine-rich repeat containing G-protein coupled receptor 4 (*Lgr4*) allele deleting the whole transmembrane domain coding region. An in vitro wound-healing scratch assay showed notably reduced keratinocyte motility in the null mice. Phalloidin staining of F-actin in the eyelid epidermis was also reduced. We also generated keratinocyte-specific *Lgr4* deficient mice, circumventing the embryonic/neonatal lethality and kidney abnormalities. Most of the conditional *Lgr4* knockout mice showed the EOB phenotype. Thus, *Lgr4* might be a novel gene class regulating cell motility.**

Keywords: LGR4; GPR48; GPCR; Gene deletion mice; EOB; Keratinocyte

1. Introduction

Lgr4 (leucine-rich repeat containing G-protein coupled receptor 4) is one of the genes identified as novel G-protein coupled receptors (GPCRs) [1,2], designated *Lgr4–Lgr8*, from an EST database with high homology to glycoprotein hormone receptors including follicle-stimulating hormone receptor (FSHR) [3], luteinizing hormone/chorionic gonadotropin receptor (LH/CGR) [4,5] and thyroid-stimulating hormone receptor (TSHR) [6].

As *Lgr4* shows high homology with FSHR, LHR and THSR, this receptor has been thought to be involved in reproductive systems. Mazerbourg et al. reported the generation of *Lgr4* gene-interrupted mice using a gene-trapped ES cell line [7], in which the expression of *Lgr4* is severely attenuated by the insertion of the β-geo gene in an enhancer trap procedure [8]. They described the neonatal lethality of the null mice, but not the cause. Previously, we generated similar *Lgr4* knockout mice by completely removing exon18, which encodes the whole transmembrane domain of *Lgr4*, in order to eliminate the chance of receptor fragment localizing at the membrane or transmitting downstream signals [9]. In those *Lgr4* knockout mice, gross hypomorphic phenotypes developed in multiple tissues and organs, and the null mice showed hypoplastic kidneys with an increased concentration of plasm creatinine, which was strongly suspected to be the cause of the neonatal/embryonic lethality.

Recently, Mendive et al. as well as Hoshii et al. reported *Lgr4* gene-trap lines exhibiting defective postnatal development of the male reproductive tract [10,11], again in contrast to the embryonic/neonatal lethality seen in our *Lgr4* knockout mice on a 129Ola × C57BL/6 hybrid background [9]. In our *Lgr4* knockout mice it appeared that complete loss of the *Lgr4* gene would induce complete embryonic/neonatal lethality. As reported in our first paper, the typical phenotype of the *Lgr4* null mutants other than the kidney aberration was eye open at birth (EOB) with 100% penetrancy, strongly suggesting reduced keratinocyte proliferation and motility. Several studies have reported a strong relationship between a reduction in keratinocyte proliferation/motility and the EOB phenotype [12,13], and it has been suggested that *Lgr4* is essential for organ development and cancer cell invasion [10,11,14]. Additionally, a close relationship between cancer cell invasion and cell motility was reported, and it is well known that organ development requires cell motility [15,16]. We therefore suspected the existence of a close relationship between *Lgr4* and cell motility, and considered that common mechanisms might cause EOB and the other abnormalities observed in *Lgr4* null mice. In the present study we focused on the EOB phenotype in relation to the keratinocyte motility of the null mice.

We provide evidence that *Lgr4* has a role in keratinocyte motility. In addition, we succeeded in dissociating the EOB phenotype, first observed in all conventional *Lgr4* KO mice, from the kidney lesions and lethality using conditional *Lgr4* knockout mice crossed with K5-Cre transgenic mice.

*Corresponding author. Fax: +81 22 717 8883.
E-mail address: knishimo@mail.tains.tohoku.ac.jp (K. Nishimori).

[1]Present address: Department of Molecular Genetics, Institute of Biomedical Sciences, Fukushima Medical University, 1 Hikarigaoka, Fukushima 960-1295, Japan.

Abbreviations: LGR, leucine-rich repeat containing G-protein coupled receptor; GPCR, G-protein coupled receptor; FSHR, follicle-stimulating hormone receptor; LH/CGR, luteinizing hormone/chorionic gonadotropin receptor; TSHR, thyroid-stimulating hormone receptor; EOB, eye-open at birth; Arbp, acidic ribosomal phosphoprotein PO

0014-5793/$32.00
doi:10.1016/j.febslet.2007.08.064

2. Materials and methods

2.1. Histology

For the eyelid histology, the heads of the mice were fixed in 4% paraformaldehyde overnight. After dehydration, they were embedded in paraffin. Paraffin blocks were sectioned at 2–5 μm thickness and stained with H&E (hematoxylin–eosin) and Phalloidin-TRITC (tetramethyl rhodamine isothiocyanate) using standard procedures.

2.2. In vitro apoptosis cell test

Sections from around the eyelids of E15.5 mice were used for the detection of apoptotic cells. Samples were processed according to the protocol of In Situ Cell Death Detection Kit (Roche, Japan).

2.3. Keratinocyte primary culture

Primary keratinocytes were isolated from neonatal mice. The epidermis was separated from the dermis with 0.8 U/ml dispase (Roche) overnight at 4 °C. Keratinocytes were dissociated by trypsin for 5 min at 34 °C and plated onto dishes precoated with collagen type I. The cells were cultured in minimum essential medium supplemented with 4% Chelex (Bio-Rad, Hercules, CA)-treated fetal calf serum epidermal growth factor (10 ng/ml; Gibco BRL), and 0.05 mM $CaCl_2$ at 34 °C in an 8% CO_2 incubator. Under these conditions, keratinocytes are maintained in an immature state characterized by active proliferation. For all the experiments, the cells were used one week after plating.

2.4. In vitro migration assay

Keratinocytes derived from each genotype of neonatal mice were cultured until confluent. After scratching with plastic tips, the distance that the keratinocyte migrated was measured every 3 h. Each sample was counted at 16 points and the average distance was calculated.

2.5. Quantitative RT-PCR

Messenger RNA derived from wild-type and *Lgr4* null mice keratinocyte was subjected to cDNA synthesis by standard procedures. Quantitative RT-PCR assays were performed with the DNA Engine Opticon System (MJ Research, Japan) with a cycling profile as follows: at 95 °C for 2 min, 39 cycles at 95 °C for 5 s, at 61.4 °C for 30 s, and at 72 °C for 30 s. The genes and primer sets are shown in the supplementary material.

2.6. Generation of keratinocyte specific Lgr4 deficient mice

To generate *Lgr4* fx/fx mice without frt-Neo-frt cassette, an initially targeted *Lgr4* mutant [9] was mated with Flp deleter [17]. Mice with the keratinocyte-specific *Lgr4* deletion were generated by breeding keratin5-Cre (K5-Cre); *Lgr4* +/− mice with *Lgr4* fx/fx mice [18]. The genetic backgrounds were C57Bl/6 × 129Ola for *Lgr4* +/− and *Lgr4* fx/fx, and C57Bl/6 × C3H for K5-Cre. Primers for *Lgr4* genotyping are shown in the supplementary material.

2.7. Statistical evaluation

All experimental data are expressed as mean S.E.M. Statistical comparisons in all the physiological and laboratory data were made among the genotype groups using ANOVA followed by Student's *t*-test for individual comparisons. *P* values of <0.05 were considered significant.

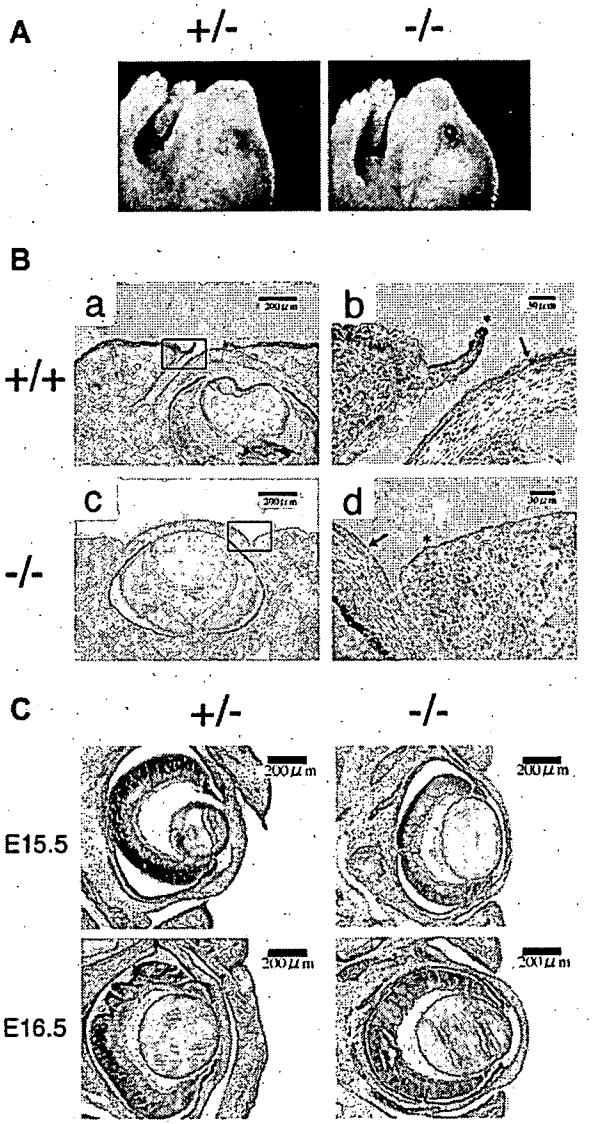

Fig. 1. *Lgr4* deficiency causes impairment in embryonic eyelid closure. (A) Left panel and right panel show morphology around eyes of *Lgr4* heterozygous (*Lgr4* +/−) and *Lgr4* null mice, respectively at postnatal day 0. (B) Eyelid sections prepared from E 15.5 wild-type (a, b) or null (c, d) mouse fetuses were immunostained with rabbit anti-LGR4 antibody (ab 12576, Abcam, USA), followed by HRP-conjugated second antibody. Asterisks show epithelial cell layer at the protruding tips of the growing eyelids, and arrows show the corneal epithelium layer. (C) Histological analysis (H&E staining) of E15.5 and E16.5 embryos.

3. Results

3.1. Lgr4 null mice show morphological abnormalities in the eyelids at E15.5

Lgr4 null mice showed some gross abnormalities. In wild-type mice during the embryonic stages E15.5 through E16.5, epithelial cells extended to the center of the eyes and finally became fused. The mice were then born with their eyelids fused, and the eyelids opened gradually by 12–14 days after birth. However, *Lgr4* null mice showed the EOB phenotype with 100% penetrance (Fig. 1A). Histological analysis of the wild-type mice followed by immunostaining showed a high expression level of *Lgr4* at the protruding tips of the eyelids and in the epithelial cells of the cornea at E15.5, but no expression was detected in the same areas of the null mice (Fig. 1B). As shown in Fig. 1C right, the eyelid closure was impaired in the null mice as compared to the heterozygous mice (Fig. 1C, left).

3.2. Proliferation and motility of keratinocytes from Lgr4 null mice

EOB has been reported as a typical phenotype reflecting keratinocyte proliferation/motility, which we then measured. No decrease in proliferating cells was detected in the eyelid epi-

thelium of the null mutants at E15.5 (data not shown). Since a reduction of the cytoplasmic accumulation of F-actin was observed with the EOB phenotype in some gene knockout studies [19,20], we stained the eyelid sections with phalloidin and found that there was less filamentous accumulation of F-actin at the margin of the eyelid epithelium, as shown in Fig. 2A. Furthermore, we examined the extent of keratinocyte proliferation in vitro using the incorporation of BrdU, but no significant difference between the wild-type and the *Lgr4* null mice was observed (date not shown). Next, the keratinocyte motility was measured by an in vitro migration assay. The lack of *Lgr4* was related to a reduction of the keratinocyte motility, and we observed a significant delay in healing 3 hours after scratching in the cells from the null mice (Fig. 2B and C). To further analyze other possible mechanisms responsible for EOB in addition to the reduced motility of the null mice, wild-type and *Lgr4* null fetuses at E15.5 were subjected to TUNEL assay to examine the extent of cell apoptosis around the eyelid tissues. However, neirther types of embryos showed any apoptotic cells (Fig. 2D).

These results suggest that the EOB observed in the null mice was not induced by an enhancement of apoptosis, and provide further evidence that *Lgr4* is a critical regulator for keratinocyte motility in the epidermal tissue of eyelids.

3.3. Quantitative RT-PCR of EOB related genes in keratinocytes from Lgr4 null mice

The disruption of *EGFR*, *EGF*, *TGF-α*, *ADAM17*, *c-jun*, *ActivinA* and *ActivinB* genes has been reported to cause EOB. We measured the expression levels of these genes in mRNA prepared from wild-type and *Lgr4* null keratinocytes, but did not detect any significant differences in their expression levels (Fig. 3). In addition, the expression level of EGFR around the eyelid at E15.5 in the null mutants was normal (Supplementary Fig. S1). The phosphorylation of EGFR around the eyelid at E15.5 was examined in wild-type and *Lgr4* null mice by immunostaining, but no significant difference was observed (date not shown). The phosphorylation of ERK and JNK of the same samples also showed no difference (Supplementary Fig.S1).

3.4. Generation of keratinocyte-specific Lgr4 deficient mice

As mentioned above, the EOB phenotype observed in *Lgr4* null mice was suspected to be closely related to reduced keratinocyte motility. We previously reported that *Lgr4* null mice showed renal hypoplasia [9]. To separate the EOB phenotype from the renal hypoplasia observed in *Lgr4* null mice, we additionally generated keratinocyte-specific *Lgr4* deficient mice (*Lgr4* conditional knockout mice) as described in Section 2

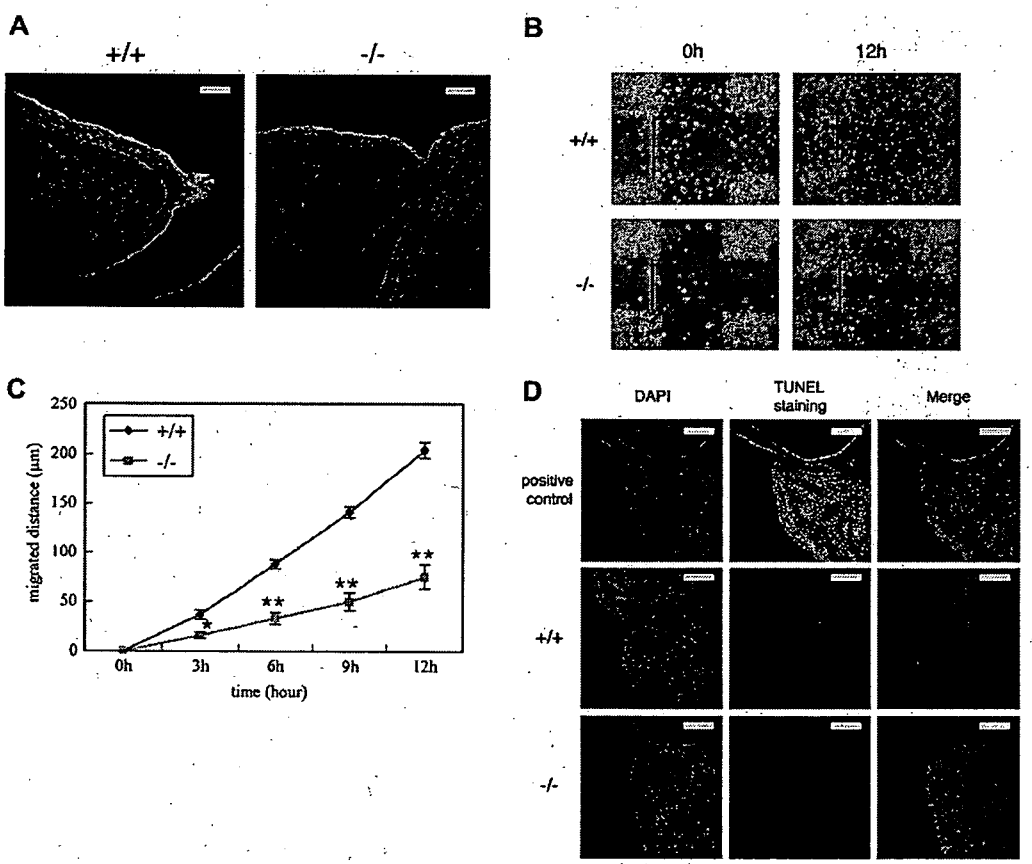

Fig. 2. EOB phenotype and impaired keratinocyte motility. (A) Coronal eye sections of E15.5 wild-type (*Lgr4* +/+) and null fetuses were stained with phalloidin-TRITC. Scale bar: 30 μm. (B) Keratinocyte motility was assessed by in vitro wound-healing scratch assay, and values representing the mean (S.E.M.; vertical bar) of 16 independent wounds are shown by a linegraph (C). (*; $P < 0.005$, **; $P < 0.001$) (D) Neither wild-type nor *Lgr4* null E15.5 fetuses showed apoptotic cells in the eyelids. Positive control is tissue treated with DNase I. Scale bar: 60 μm.

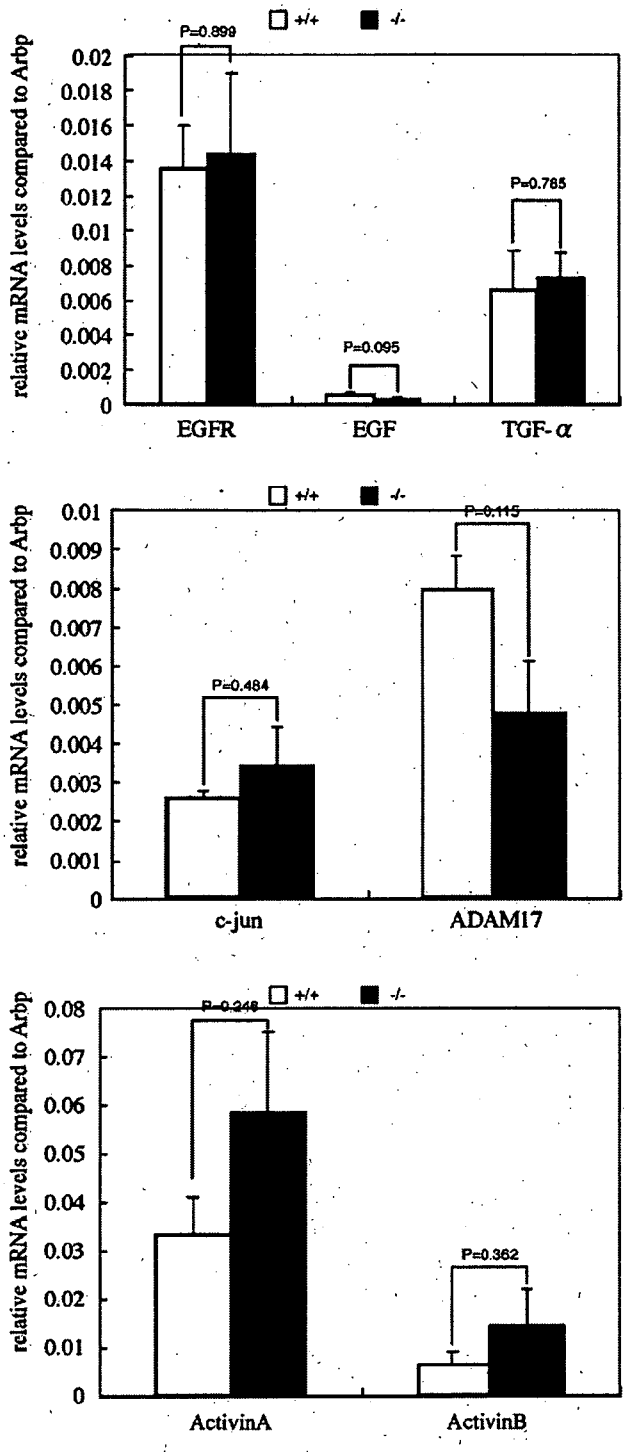

Fig. 3. Quantitative RT-PCR for cell motility-related genes. EGFR, EGF, TGF-α, c-jun, ADAM17, ActivinA and ActivinB mRNA levels in keratinocyte derived from *Lgr4* wild-type and null mice (P0) were quantified (all bars; $n = 3$). Error bars represent ± S.E.M.

(Supplementary Fig. S2A and B). The keratinocyte-specific deletion of *Lgr4* gene in *Lgr4* conditional knockout mice was confirmed by RT-PCR (Fig. 4A). The *Lgr4* conditional knockout mice were spared the embryonic/neonatal lethality (data not shown) and almost all of them showed the EOB phenotype (Fig. 4B and C). The body size and weight of several organs including the kidneys and liver were all reduced in *Lgr4* null mice [9], whereas those of the conditional knockout mice were all normal (Fig. 4D and E).

4. Discussion

In this report, we demonstrated an abnormality in the motility of keratinocytes and the EOB phenotype in *Lgr4* null mice. It is known that, during normal mouse development, the epithelial cells on the protruding tips of both the upper and lower eyelids migrate along the surface of the cornea and fuse with each other by E16.5 [12]. This suggests that EOB could be due to a defect in prenatal eyelid extension. EOB has been reported as a typical phenotype in mutant mice lacking several genes affecting epithelial cell proliferation and motility [12,13]. The genes whose deletion results in EOB include transcription factors controlling cell proliferation (c-jun [21,22]), growth factors (FGF10 [23], HB-EGF [20,24], TGF-α [25], ActivinB [26]) and their receptors (EGFR [27]), and related cytoplasmic factors functioning in signal transduction pathways (MEKK1 [28,29], JNK [30]). Xia et al. reviewed the signaling pathways required for embryonic eyelid closure in normal developmental stages and classified these into two major signaling pathways, TGFβ/activin-MEKK1-JNK/p38 and TGF-α/EGFR-ERK [13]. Our data strongly suggest that *Lgr4* plays a critical role in regulating the formation of eyelids in the embryonic stage and that it contributes to epithelial cell motility. In addition, epidermal wound-healing activity [21,27] and tumorigenesis require epithelial cell motility [29]. Although the downstream signaling mechanisms of *Lgr4* are not clear, we speculate that a novel signaling pathway exists in keratinocytes to regulate the cell motility.

We generated *Lgr4* conditional knockout mice that were spared the embryonic/neonatal lethality, reduced body weight and renal hypoplasia observed in *Lgr4* null mice, and were born with a mendelian distribution. However, almost all of these mice showed the EOB phenotype. These results strongly suggest that the keratinocyte aberration shown by *Lgr4* null mice was not induced by renal hypoplasia.

The observed impairment in keratinocyte motility may suggest that *Lgr4* controls the cell motility of keratinocytes. In this context, elucidating the precise role of *Lgr4* along with its cognate ligand would advance the knowledge of the epithelial cell motility mechanism. Interestingly, one of our *Lgr4* null mice survived for more than 40 days, showing turbid corneas in addition to various defects. Microscopic observation of the cornea showed many stripes (data not shown), and we presume that the degeneration of the cornea, including wounds, resulted from excoriation by the floor material in the cage because of the EOB. However, immunostaining of the eye tissue clearly showed positive staining at the cornea in the wild-type mice in addition to the signal at the protruding tips of the eyelid (Fig. 1B). This result also suggests the possibility that the turbid cornea observed in null mice might be caused by a deficiency of the *Lgr4* gene. Therefore, a cornea-specific deletion of *Lgr4* will be required to study further the function of *Lgr4* in the development, growth and maintenance of the cornea tissue. To our knowledge, there are no published reports of EOB caused by a deficiency of GPCR genes. In addition, in the other reports on the generation of *Lgr4* mutants (by insertion of a gene cassette carrying a splice acceptor into to an intron of

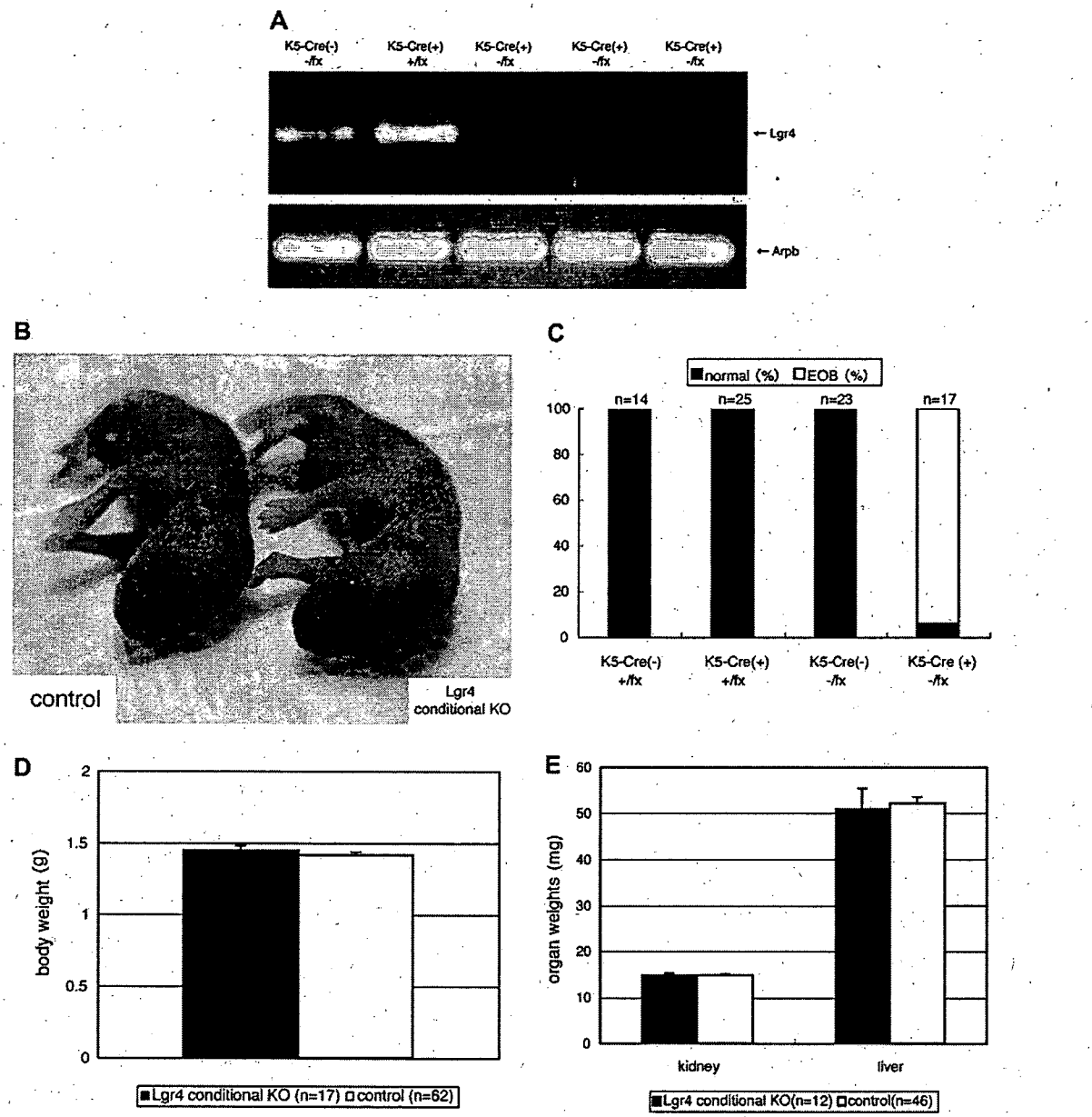

Fig. 4. Characteristics of *Lgr4* conditional knockout mice. (A) RT-PCR for *Lgr4* showed no expression of *Lgr4* mRNA in keratinocytes. Primer sets are shown in the supplementary material. (B) *Lgr4* conditional knockout mice show the typical EOB phenotype. (C) As in the case of *Lgr4* null mice, almost all of the *Lgr4* conditional knockout mice show the EOB phenotype. The body weight (D) and the organ weight of the liver and kidneys (E) of *Lgr4* conditional knockout mice are all within normal ranges.

the gene) on several genetic backgrounds [8,10,11], the EOB phenotype of the null mice was not described except in one abstract for a poster presentation [31]. Nevertheless, we predicted that *Lgr4* and its unidentified ligand(s) would likely be related to regulatory mechanisms controlling the development and maintenance of epidermal tissue including that of the eyelid.

In conclusion, we generated two mouse models, one with a complete deletion of the *Lgr4* function and another with a conditional *Lgr4* knockout, and provide evidence that *Lgr4* is involved in keratinocyte motility affecting eyelid formation. Adult conditional *Lgr4* knockout mice will be a useful tool for examining the *Lgr4* function in keratinocytes.

Acknowledgements: We would like to thank Dr. J. Takeda for providing us the K5 Cre TG mice, and Dr. M. Kitagawa for valuable discussion. This research was supported in part by a Grants-in-Aid for Exploratory Research (#17659251) from the Ministry of education, Culture, Sports, Science and Technology of Japan, and by a donation from Kureha Corporation.

Appendix A. Supplementary data

Supplementary data associated with this article can be found, in the online version, at doi:10.1016/j.febslet.2007.08.064.

References

[1] Hsu, S.Y., Liang, S.G. and Hsueh, A.J. (1998) Characterization of two LGR genes homologous to gonadotropin and thyrotropin receptors with extracellular leucine-rich repeats and a G protein-coupled, seven-transmembrane region. Mol. Endocrinol. 12, 1830–1845.

[2] Loh, E.D., Broussard, S.R., Liu, Q., Copeland, N.G., Gilbert, D.J., Jenkins, N.A. and Kolakowski Jr., L.F. (2000) Chromosomal localization of GPR48, a novel glycoprotein hormone receptor like GPCR, in human and mouse with radiation hybrid and interspecific backcross mapping. Cytogenet. Cell. Genet. 89, 2–5.

[3] Baker, P.J., Pakarinen, P., Huhtaniemi, I.T., Abel, M.H., Charlton, H.M., Kumar, T.R. and O'Shaughnessy, P.J. (2003) Failure of normal Leydig cell development in follicle-stimulating hormone (FSH) receptor-deficient mice, but not FSHbeta-deficient mice: role for constitutive FSH receptor activity. Endocrinology 144, 138–145.

[4] Huhtaniemi, I., Zhang, F.P., Kero, J., Hamalainen, T. and Poutanen, M. (2002) Transgenic and knockout mouse models for the study of luteinizing hormone and luteinizing hormone receptor function. Mol. Cell. Endocrinol. 187, 49–56.

[5] Zhang, F.P., Poutanen, M., Wilbertz, J. and Huhtaniemi, I. (2001) Normal prenatal but arrested postnatal sexual development of luteinizing hormone receptor knockout (LuRKO) mice. Mol. Endocrinol. 151, 72–183.

[6] Postiglione, M.P., Parlato, R., Rodriguez-Mallon, A., Rosica, A., Mithbaokar, P., Maresca, M., Marians, R.C., Davies, T.F., Zannini, M.S., De Felice, M. and Di Lauro, R. (2002) Role of the thyroid-stimulating hormone receptor signaling in development and differentiation of the thyroid gland. Proc. Natl. Acad. Sci. USA 99, 15462–15467.

[7] Leighton, P.A., Mitchell, K.J., Goodrich, L.V., Lu, X., Pinson, K., Scherz, P., Skarnes, W.C. and Tessier-Lavigne, M. (2001) Defining brain wiring patterns and mechanisms through gene trapping in mice. Nature 410, 174–179.

[8] Mazerbourg, S., Bouley, D.M., Sudo, S., Klein, C.A., Zhang, J.V., Kawamura, K., Goodrich, L.V., Rayburn, H., Tessier-Lavigne, M. and Hsueh, A.J. (2004) Leucine-rich repeat-containing, G protein-coupled receptor 4 null mice exhibit intrauterine growth retardation associated with embryonic and perinatal lethality. Mol. Endocrinol. 18, 2241–2254.

[9] Kato, S., Matsubara, M., Matsuo, T., Mohri, Y., Kazama, I., Hatano, R., Umezawa, A. and Nishimori, K. (2006) Leucine-rich repeat-containing G protein-coupled receptor-4 (LGR4, Gpr48) is essential for renal development in mice. Nephron Exp. Nephrol. 104, e63–e75.

[10] Mendive, F., Laurent, P., Van Schoore, G., Skarnes, W., Pochet, R. and Vassart, G. (2006) Defective postnatal development of the male reproductive tract in LGR4 knockout mice. Dev. Biol. 290, 421–434.

[11] Hoshii, T., Takeo, T., Nakagata, N., Takeya, M., Araki, K. and Yamamura, K. (2007) LGR4 regulates the postnatal development and integrity of male reproductive tracts in mice. Biol. Reprod. 76, 303–313.

[12] Xia, Y. and Karin, M. (2004) The control of cell motility and epithelial morphogenesis by Jun kinases. Trends Cell. Biol. 14, 94–101.

[13] Xia, Y. and Kao, W.W. (2004) The signaling pathways in tissue morphogenesis: a lesson from mice with eye-open at birth phenotype. Biochem. Pharmacol. 68, 997–1001.

[14] Gao, Y., Kitagawa, K., Hiramatsu, Y., Kikuchi, H., Isobe, T., Shimada, M., Uchida, C., Hattori, T., Oda, T., Nakayama, K., Nakayama, K.I., Tanaka, T., Konno, H. and Kitagawa, M. (2007) Up-regulation of GPR48 induced by down-regulation of p27Kip1 enhances carcinoma cell invasiveness and metastasis. Cancer Res. 66, 11623–11631.

[15] Keller, R. (2002) Shaping the vertebrate body plan by polarized embryonic cell movements. Science 298, 1950–1954.

[16] Sahai, E. (2005) Mechanisms of cancer cell invasion. Curr. Opin. Genet. Dev. 15, 87–96.

[17] Rodriguez, C.I., Buchholz, F., Galloway, J., Sequerra, R., Kasper, J., Ayala, R., Stewart, A.F. and Dymecki, S.M. (2000) High-efficiency deleter mice show that FLPe is an alternative to Cre-loxP. Nat. Genet. 25 (2), 139–140.

[18] Tarutani, M., Itami, S., Okabe, M., Ikawa, M., Tezuka, T., Yoshikawa, K., Kinoshita, T. and Takeda, J. (1997) Tissue-specific knockout of the mouse Pig-a gene reveals important roles for GPI-anchored proteins in skin development. Proc. Natl. Acad. Sci. USA 94, 7400–7405.

[19] Mine, N., Iwamoto, R. and Mekada, E. (2005) HB-EGF promotes epithelial cell migration in eyelid development. Development 132, 4317–4326.

[20] Shimizu, Y., Thumkeo, D., Keel, J., Ishizaki, T., Oshima, H., Oshima, M., Noda, Y., Matsumura, F., Taketo, M.M. and Narumiya, S. (2005) ROCK-I regulates closure of the eyelids and ventral body wall by inducing assembly of actomyosin bundles. J. Cell Biol. 168, 941–953.

[21] Li, G., Gustafson-Brown, C., Hanks, S.K., Nason, K., Arbeit, J.M., Pogliano, K., Wisdom, R.M. and Johnson, R.S. (2003) c-Jun is essential for organization of the epidermal leading edge. Dev. Cell. 4, 865–877.

[22] Zenz, R., Scheuch, H., Martin, P., Frank, C., Eferl, R., Kenner, L., Sibilia, M. and Wagner, E.F. (2003) c-Jun regulates eyelid closure and skin tumor development through EGFR signaling. Dev. Cell. 4, 879–889.

[23] Tao, H., Shimizu, M., Kusumoto, R., Ono, K., Noji, S. and Ohuchi, H. (2005) A dual role of FGF10 in proliferation and coordinated migration of epithelial leading edge cells during mouse eyelid development. Development 132, 3217–3230.

[24] Shirakata, Y., Kimura, R., Nanba, D., Iwamoto, R., Tokumaru, S., Morimoto, C., Yokota, K., Nakamura, M., Sayama, K., Mekada, E., Higashiyama, S. and Hashimoto, K. (2005) Heparin-binding EGF-like growth factor accelerates keratinocyte migration and skin wound healing. J. Cell. Sci. 118, 2363–2370.

[25] Luetteke, N.C., Qiu, T.H., Peiffer, R.L., Oliver, P., Smithies, O. and Lee, D.C. (1993) TGF alpha deficiency results in hair follicle and eye abnormalities in targeted and waved-1 mice. Cell 73, 263–278.

[26] Vassalli, A., Matzuk, M.M., Gardner, H.A., Lee, K.F. and Jaenisch, R. (1994) Activin/inhibin beta B subunit gene disruption leads to defects in eyelid development and female reproduction. Genes Dev. 8, 414–427.

[27] Miettinen, P.J., Berger, J.E., Meneses, J., Phung, Y., Pedersen, R.A., Werb, Z. and Derynck, R. (1995) Epithelial immaturity and multiorgan failure in mice lacking epidermal growth factor receptor. Nature 376, 337–341.

[28] Yujiri, T., Ware, M., Widmann, C., Oyer, R., Russell, D., Chan, E., Zaitsu, Y., Clarke, P., Tyler, K., Oka, Y., Fanger, G.R., Henson, P. and Johnson, G.L. (2000) MEK kinase 1 gene disruption alters cell migration and c-Jun NH2-terminal kinase regulation but does not cause a measurable defect in NF-kappa B activation. Proc. Natl. Acad. Sci. USA 97, 7272–7277.

[29] Zhang, L., Wang, W., Hayashi, Y., Jester, J.V., Birk, D.E., Gao, M., Liu, C.Y., Kao, W.W., Karin, M. and Xia, Y. (2003) A role for MEK kinase 1 in TGF-beta/activin-induced epithelium movement and embryonic eyelid closure. EMBO J. 22, 4443–4454.

[30] Weston, C.R., Wong, A., Hall, J.P., Goad, M.E., Flavell, R.A. and Davis, R.J. (2004) The c-Jun NH2-terminal kinase is essential for epidermal growth factor expression during epidermal morphogenesis. Proc. Natl. Acad. Sci. USA 101, 14114–14119.

[31] Hoshii, T., Sakumura, Y., Araki, M., Araki, K. and Yamamura, K. (2005) Analysis of abnormality in eye lid formation in LGR4 mutant mice. In: Proceedings of the 39th Annual Meeting of Japanese Society of Developmental Biologists, 1P031.

Available online at www.sciencedirect.com
ScienceDirect
Journal of Chromatography A, 1160 (2007) 263–269
JOURNAL OF CHROMATOGRAPHY A
www.elsevier.com/locate/chroma

Study on the quality control of cell therapy products Determination of *N*-glycolylneuraminic acid incorporated into human cells by nano-flow liquid chromatography/Fourier transformation ion cyclotron mass spectrometry

Noritaka Hashii [a,b], Nana Kawasaki [a,b,*], Yukari Nakajima [a,b], Masashi Toyoda [c], Yoko Katagiri [c], Satsuki Itoh [a], Akira Harazono [a], Akihiro Umezawa [c], Teruhide Yamaguchi [a]

[a] *Division of Biological Chemistry and Biologicals, National Institute of Health Sciences, 1-18-1 Kamiyouga, Setagaya-ku, Tokyo 158-8501, Japan*
[b] *Core Research for Evolutional Science and Technology (CREST) of Japan Science and Technology Agency (JST), 4-1-8 Hon-cho, Kawaguchi, Saitama 332-0012, Japan*
[c] *National Research Institute for Child Health and Development, 2-10-1 Okura, Setagaya-ku, Tokyo 157-8535, Japan*

Received 6 February 2007; received in revised form 16 May 2007; accepted 21 May 2007
Available online 25 May 2007

Abstract

N-Glycolylneuraminic acid (NeuGc), an acidic nine-carbon sugar, is produced in several animals, such as cattle and mice. Since human cells cannot synthesize NeuGc, it is considered to be immunogenic in humans. Recently, NeuGc contamination was reported in human embryonic stem cells cultured with xenogeneic serum and cells, suggesting that possibly NeuGc may harm the efficacy and safety of cell therapy products. Sialic acids have been determined by derivatization with 1,2-diamino-4,5-methylenedioxybenzene (DMB) followed by liquid chromatography/mass spectrometry (LC/MS) and liquid chromatography/tandem mass spectrometry (LC/MS/MS); however, the limited availability of cell therapy products requires more sensitive and specific methods for the quality test. Here we studied the use of nano-flow liquid chromatography/Fourier transformation ion cyclotron resonance mass spectrometry (nanoLC/FTMS) and nanoLC/MS/MS for NeuGc-specific determination at a low femtomole level. Using our method, we found NeuGc contamination of the human cell line (HL-60RG cells) cultured with human serum. Our method needs only 2.5×10^3 cells for one injection and would be applicable to the determination of NeuGc in cell therapy products.

Keywords: *N*-Glycolylneuraminic acid; Nano-flow liquid chromatography; Fourier transformation ion cyclotron mass spectrometry; Cell therapy products

1. Introduction

Sialic acids are a family of acidic nine-carbon sugars found in the non-reducing terminal of *N*-linked and *O*-linked oligosaccharides of glycoproteins and glycolipids [1,2]. There are more than 30 members with different substitutions on the amino group at carbon 5 and on hydroxyl groups at carbons 4, 7, 8 and 9 [2–8]. *N*-Glycolylneuraminic acid (NeuGc), a 5-*N*-glycolylated sialic acid, is produced in several animals, such as cattle, horses, mice and rats [9]. Since human cells cannot synthesize NeuGc due to mutation of the cytidine monophospho (CMP)-*N*-acetylneuraminic acid (NeuAc) hydroxylase gene [10,11], NeuGc is considered to be antigenic and to induce immunoreaction in humans [4,12,13].

Advances in biotechnology and cell culture techniques make it possible to administer human and animal cells directly to patients as cell therapy products. In cell therapy and tissue engineering, human embryonic stem (ES) cells are expected to be useful for the treatment of many diseases. Recently, it was reported that NeuGc is incorporated into ES cells from human and mouse feeder cells and cultivation media containing xenogeneic serum, such as fetal calf serum (FCS) [14,15]. Since NeuGc is a foreign component in humans, it is feared that NeuGc may harm the efficacy and safety of cell therapy products. To

* Corresponding author. Tel.: +81 3 3700 9074; fax: +81 3 3700 9084.
E-mail address: nana@nihs.go.jp (N. Kawasaki).

0021-9673/$ – see front matter © 2007 Elsevier B.V. All rights reserved.
doi:10.1016/j.chroma.2007.05.062

assess the adverse effects of NeuGc, it is necessary to quantify NeuGc in cell therapy products.

Sialic acids have been determined by labeling with 1,2-diamino-4,5-methylenedioxybenzene (DMB) followed by conventional high-performance liquid chromatography (HPLC) with fluorescent detection [16–20]. The femtomole level of sialic acid can be determined by fluorescent detection [19]. The use of liquid chromatography/mass spectrometry (LC/MS) and liquid chromatography/tandem mass spectrometry (LC/MS/MS) has more advantage in the identification of sialic acid species [18,20–22]. The derivatization of sialic acids with DMB has advantages of good separation of NeuGc from NeuAc in chromatography and enhancement of ionization efficiency in MS. However, more sensitive and specific methods are desired for the quality control of cell therapy products, since in many case only a low number of cell products, approximately 1×10^6 to 1×10^8, should be available for quality tests.

In this study, we studied the use of nano-flow liquid chromatography/Fourier transformation ion cyclotron resonance mass spectrometry (nanoLC/FTMS) and LC/MS/MS to achieve the sensitive and specific determination of NeuGc. The potential of the method for quality testing of cell therapy products was evaluated using substrain of human promyelocytic leukemia HL-60 cells (HL-60RG cells) as model cells. Using this method, we determined NeuGc in membrane fractions from HL-60RG cells cultured with FCS, human serum and serum-free medium.

2. Experimental

2.1. Materials

NeuGc and NeuAc were purchased from Nacalai Tesque (Kyoto, Japan). FCS and normal human serum were purchased from Dainippon Sumitomo Pharma (Osaka, Japan). RPMI1640 medium and ASF104 medium were purchased from Sigma-Aldrich (St. Louis, MO, USA) and Ajinomoto (Tokyo, Japan), respectively.

2.2. Cell culture

Substrain of human promyelocytic leukemia HL-60 cells (HL-60RG cells, JCRB Cellbank, Osaka, Japan) was cultured in RPMI1640 medium supplemented with 10% FCS, 100 unit/ml of penicillin and 100 μg/ml of streptomycin under a humidified atmosphere of 95% air and 5% CO_2 at 37 °C. HL-60RG cells were replaced at 2×10^5 cells/100 mm dish in RPMI1640 medium supplemented with 10% FCS or 10% normal human serum, and in serum-free ASF104 medium. The media were replaced four times, and semi-confluent growth cells were harvested.

2.3. Fractionation of the membrane fraction

The cells were washed in phosphate buffer saline (PBS) supplemented with protease inhibitors (protease inhibitor mix solution, Wako, Tokyo, Japan) three times. The washed cells (1×10^6) were suspended in 100 μl of 0.25 M sucrose/10 mM Tris–HCl buffer (pH 7.4) containing protease inhibitors, and sonicated at 4 °C for 30 s, two times (40W, Bioruptor UCW-201, Tosyoudenki, Kanagawa, Japan). After the nuclei were removed by centrifugation at 4 °C, 450 × *g* for 10 min, the mitochondria and lysosome fractions were removed by re-centrifugation at 4 °C, 20,000 × *g* for 10 min. The membrane fractions were precipitated by ultracentrifugation at 4 °C, 100,000 × *g* for 60 min. The membrane fractions were washed in 100 μl of 150 mM ammonium acetate buffer (pH 7.4) and recovered by re-ultracentrifugation.

2.4. Derivatization of NeuGc and NeuAc with DMB reagent

The membrane fractions were sonicated in 250 μl of H_2O and then incubated with 250 μl of 4 M acetic acid (final concentration, 2 M) at 80 °C for 3 h. The released sialic acids were passed though a solid-phase extraction cartridge (SepPak C-18, Waters, Milford, MA, USA) with 2 ml of H_2O, dried under vacuum, and resolved in 50 μl of H_2O. The solution was incubated with DMB according to the manufacturer's instruction (Takara, Tokyo, Japan), and the reaction mixture was applied on a solid-phase extraction cartridge (Envi-Carb C, Supelco, Bellefonte, PA, USA). After washing the cartridge with 2.5 ml of 5 mM ammonium acetate (pH 9.6) for desalting, the DMB-labeled sialic acids were eluted with 3 ml of 45% acetonitrile/5 mM ammonium acetate (pH 9.6). The collected fraction was freeze dried.

2.5. nanoLC/FTMS

DMB-labeled sialic acids were separated by HPLC using Paradigm MS4 (Michrom BioResource, Auburn, CA, USA) equipped with a reversed-phase C18 column (Magic C18, 50 mm × 0.1 mm, 3 μm, Michrom BioResource, Auburn, CA, USA). Elution was achieved using 0.1% formic acid/2% ace-

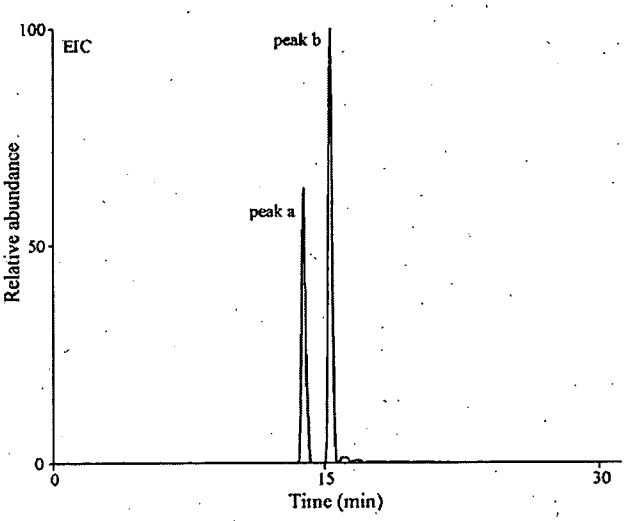

Fig. 1. EIC at *m/z* 426.13–426.17 and *m/z* 442.12–442.16 obtained by SIM (*m/z* 400–450) of DMB-NeuGc and DMB-NeuAc in the positive ion mode.